Morphology and line tension of liquid films adsorbed on chemically structured substrates

W. Koch and S. Dietrich
Fachbereich Physik, Bergische Universität Wuppertal, D-42097 Wuppertal, Federal Republic of Germany

M. Napiórkowski
Instytut Fizyki Teoretycznej, Uniwersytet Warszawski, Hoża 69, 00-681 Warszawa, Poland
(Received 23 September 1994)

On the basis of a microscopic density-functional theory for inhomogeneous fluids we investigate the structure of liquidlike films adsorbed on laterally inhomogeneous, flat substrates that consist of two adjacent halves occupied by different chemical species. All atomic interactions are taken to be long ranged. The corresponding integral equations for the equilibrium density profile are solved numerically. The mean position of the interface between the liquidlike adsorbed film and the bulk vapor phase displays van der Waals tails; their amplitudes are calculated analytically for complete and critical wetting. As an approximation we recover the standard phenomenological approach for the profile of the mean interface position whose quantitative behavior turns out to fail drastically as compared with that obtained from the appropriate nonlocal theory. The shape of the interface profile gives rise to a line tension that diverges logarithmically for complete wetting transitions and exhibits a cusplike singularity close to critical wetting transitions.

PACS number(s): 68.45.Gd, 68.10.−m, 82.65.Dp

I. INTRODUCTION

Two phases α and γ of one-component condensed matter can coexist in thermal equilibrium over a certain range of temperature T and for specific values $\mu_0(T)$ of the chemical potential μ. Under these conditions and in the presence of appropriate boundary conditions an α-γ interface can form. If upon a change of the thermodynamical parameters a third phase β becomes stable, it may wet the α-γ interface leading to two separated interfaces α-β and β-γ. The particular case in which the phase α happens to be a flat, structureless, and inert wall wetted by a liquid β in coexistence with its vapor γ has been studied extensively (for reviews see, e.g., Refs. [1–3]). The wetting transition is characterized by the growth of the thickness of the liquidlike layer. If this growth is induced upon approaching the liquid-vapor coexistence line from the gas side, this transition is called complete wetting. If the thermodynamic state is changed along the liquid-vapor coexistence line of the fluid, the continuous growth of the film thickness is called second-order or critical wetting, whereas a discontinuous jump from a microscopic to a macroscopic value of the film thickness is called first-order wetting. The value of the temperature at which the film thickness diverges defines the wetting temperature T_w. The different kinds of wetting behavior can be transparently understood by introducing the concept of the effective interface potential, which is defined as the value of the wall-gas surface tension under the constraint of a prescribed thickness of the liquidlike layer [4,5].

However, real substrate surfaces exhibit various geometrical or chemical imperfections that destroy the translational invariance in the lateral directions. On the basis of both phenomenological and microscopic theories the *geometrical* effects of such heterogeneities on the morphology of liquidlike adsorbed films have been studied intensively, e.g., for fractal [6–9], rough [10], corrugated [11–14], or wedgelike substrates [15–20]. On the other hand, *chemical* inhomogeneities have been investigated to a much lesser extent.

To our knowledge the only study of that sort is contained in Ref. [21] in which—within a phenomenological approach—the authors considered the adsorption of thin liquid films on a flat substrate that consists of two halves occupied by different species. This analysis dates back to 1976, before the theory of wetting transitions was formulated and before modern density-functional theories for the microscopic description of inhomogeneous fluids were fully developed. The additional knowledge that has been accumulated since then allows us to shed light on this problem and to obtain a refined picture.

In the meantime chemically structured substrates have not only attracted recent academic interest, but they also have attained technological importance. Molecular surfactants render oil and water miscible by stabilizing interfaces between them and thus giving rise to micell formation. Normally surfactants are so densely packed at these interfaces that they prohibit, e.g., ion diffusion through it. This blocking can be avoided by using instead artificial amphiphilic particles called Janus beads, which are glass spheres with a diameter ranging between 50 and 100 μm whose surfaces are treated chemically in such a way that one hemisphere is rendered hydrophobic whereas the other is hydrophilic. Janus beads exhibit the specific behavior of anchoring at a fluid interface along their equator. Inspired by de Gennes [22], several investigations of the static [23–26] and dynamic [27–29] wetting properties of these objects have been carried out. Our present study is supposed to provide some microscopic

insight into the behavior of Janus beads insofar as one is concerned with the morphology of thin liquids films exposed to a substrate with spatially varying and competing wetting properties. However, as a caveat one should keep in mind that the system we are considering differs from that of the Janus beads in two aspects: First, our surface is flat and second, the chemical composition of the two substrate halves differs even deep in the bulk of the substrate and not only on its surface. In view of the large diameter of the Janus beads compared with typical wetting thicknesses of about several hundred angstroms, the curvature effects on wetting (see Sec. X B in Ref. [2]) will be only minor. The second difference seems to be more important.

Finally, we would like to mention that there is a rich variety of even more complicated chemical patterns of substrate surfaces that are of current interest. They include adsorption on columnar structures [30], hole formation in coated films induced by the presence of nonwetting defects [31], monolayer adsorption on energetically heterogeneous surfaces [32], and selective vapor-phase deposition on patterned substrates [33]. If the fluid is confined by *two* parallel plates, a liquidlike phase will form for values of the pressure below that of saturation. This capillary condensation will also be influenced by lateral chemical (or geometrical) heterogeneities of the confining substrates [34,35].

Figure 1 describes the system we are considering. The substrate fills the half space $\Lambda_w=\Lambda_+\cup\Lambda_-$ whereby the quarter spaces $\Lambda_\pm=\{\mathbf{r}=(x,y,z)\in\mathbb{R}^3|x\gtrless 0,z<0\}$ are occupied by two chemically different species. With this choice the system is translationally invariant along the y direction, which is parallel to the plane of contact $x=0$ between the different substrate species. In Sec. II we introduce and specify the grand-canonical density functional and the interaction potentials that we use throughout this work. The systematic decomposition of the free-energy functional into bulk, surface, and line contributions leads us to an explicit microscopic expression for the line tension τ that is associated with the variation of the fluid density in the lateral direction x. The minimization of the line contribution with respect to the number density distribution renders an integral equation for the equilibrium density configuration $\rho(x,z)$ that is solved numerically. Since this requires a substantial numerical effort and in practice puts a limit on the thickness of wetting films one can study, in Sec. III we restrict our analysis to low temperatures and thus to density configurations that vary steplike in the vertical direction at $z=l(x)$ between the bulk vapor density $\rho_g(T,\mu)$ and the liquid density $\rho_l(T,\mu=\mu_0(T))$. The resulting equation for the profile $l(x)$ of the interface position exhibits also a nonlocal character. Whereas the full profile $l(x)$ has again to be computed numerically (requiring now a reduced numerical effort), we have been able to determine the asymptotic behavior of $l(x)$ for large $|x|$ analytically. In Sec. IV we compare our results with those obtained from the standard phenomenological and local effective Hamiltonian that follows from the aforementioned nonlocal expression by applying a systematic gradient expansion. It turns out that the asymptotic features of $l(x)$ for large $|x|$ are the same; however, the local approximation exaggerates drastically the variation of $l(x)$ close to the transition region at $x=0$. The local form of the effective interface Hamiltonian allows us to determine the singular behavior of line tension of the system analytically for the particularly interesting case that the more attractive substrate is wetted whereas the other is not. Section V summarizes our results and contains a discussion including a comparison of our findings with recent results for the behavior of line tensions close to wetting transitions [36]. Details of the explicit forms of bulk, surface, and line contributions to the grand-canonical free-energy functional within the various approximation schemes are given in Appendixes A and B.

II. DENSITY-FUNCTIONAL APPROACH

Our analysis is based on a simple local version of a mean field, grand-canonical density functional for inhomogeneous fluids [37] (for its application to standard wetting phenomena and its limitations see, e.g., Refs. [1–3]):

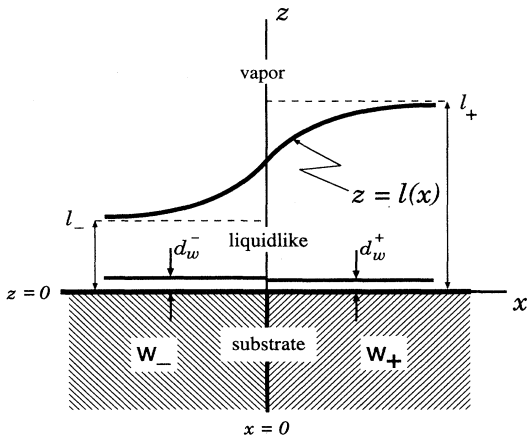

FIG. 1. Qualitative description of the system under consideration. The vapor phase is exposed to a substrate filling the half space $z\leq 0$. $z=0$ denotes the position of the nuclei of the top substrate layer. The lattice structure of the substrate in the lateral directions x and y is ignored. The substrate consists of the two quarter spaces Λ_- and Λ_+ with $z<0$, and $x<0$ and $x>0$, respectively, occupied by different species indicated by the different hatching. The system is translationally invariant in the y direction. A liquidlike film, in thermal equilibrium with the vapor phase, is adsorbed on the substrate. $z=l(x)$ denotes the position of the liquid-vapor interface. If $\rho(x,z)$ denotes the number density of the fluid, we adopt as the definition of the interface position $\rho(x,z=l(x))=(\rho_l+\rho_g)/2$, where ρ_l and ρ_g are the liquid and vapor bulk number densities at two-phase coexistence. The substrate w_- is less attractive than the substrate w_+ so that $l_+>l_-$, where $l_\pm=l(x\to\pm\infty)$ denotes the thickness of the wetting film if the vapor phase is exposed to a *half* space filled with the substrate $w_\pm$ under the same thermodynamic conditions. d_w^- and d_w^+ denote excluded volumes due to the repulsive parts of the substrate potentials [2]. In most cases the less attractive substrate will have the larger d_w.

$$\Omega[\{\rho(\mathbf{r})\};T,\mu;\{w(\mathbf{r})\},\{V(\mathbf{r})\}]$$
$$=\int_{\Lambda_f} d^3r\, f_{\mathrm{HS}}(\rho(\mathbf{r}),T)$$
$$+\tfrac{1}{2}\int_{\Lambda_f} d^3r \int_{\Lambda_f} d^3r'\,\tilde{w}(|\mathbf{r}-\mathbf{r}'|)\rho(\mathbf{r})\rho(\mathbf{r}')$$
$$+\int_{\Lambda_f} d^3r\,\rho(\mathbf{r})[V(\mathbf{r})-\mu]\ . \qquad (2.1)$$

The integrations in Eq. (2.1) are taken over the space Λ_f occupied by the fluid. The interaction between the fluid particles is assumed to be given by a spherically symmetric pair potential $w(r)$, which is separated into a long-range attractive part and a short-range repulsive part. $\tilde{w}(r)$ represents the attractive part that, at large distances, decays like r^{-6} and at short distances is consistent with the Weeks-Chandler-Andersen (WCA) prescription [38]. The repulsive part of the potential w is mapped onto an effective hard sphere interaction potential. The first term in Eq. (2.1) is the contribution to the free-energy functional from the repulsive part of the potential treated within the local density approximation; $f_{\mathrm{HS}}(\rho,T)$ denotes the Helmholtz free-energy density of a homogeneous system of hard spheres with a number density ρ. μ is the chemical potential and $V(\mathbf{r})$ is the substrate potential, which at large distances is attractive and decays $\sim z^{-3}$, where z is the distance from the substrate surface. Explicit forms of the interaction potentials $\tilde{w}$ and V are given below [cf. Eqs. (2.13) and (2.17)–(2.19)].

Since the substrate potential $V(\mathbf{r})=V(x,z)$ does not depend on y and because the translational invariance in that direction is not broken by boundary conditions, one has $\rho(\mathbf{r})=\rho(x,z)$ (see Fig. 2). Starting from a finite system size $L_x\times L_y\times L_z$ for the fluid volume Λ_f a systematic analysis of the size dependences leads to the following decomposition of the grand-canonical density-functional given by Eq. (2.1) into its bulk (Ω_b), surface (Ω_s), and line (Ω_l) contributions, which is valid for all trial functions $\rho(x,z)$ that approach their asymptotic values rapidly enough:

$$\lim_{L_y\to\infty}\frac{1}{L_y}\Omega[\{\rho(x,z)\};T,\mu]$$
$$=L_xL_z\Omega_b(\rho_g,T,\mu)+L_z\Omega_s^{\perp}(\rho_g,T,\mu)$$
$$+L_x\Omega_s^{\parallel}[\{\rho_+(z),\rho_-(z)\};\rho_l,\rho_g,T,\mu]$$
$$+\Omega_l[\{\rho(x,z)\};\rho_l,\rho_g,T,\mu]+O\left[\frac{1}{L_x},\frac{1}{L_z}\right]\ . \qquad (2.2)$$

Those contributions to Ω that scale as L_xL_y are proportional to $\Omega_s^{\parallel}$, whereas those that scale as L_yL_z are proportional to $\Omega_s^{\perp}$. One should note that Eq. (2.2) includes artificial surface and line contributions due to interfaces with the vacuum generated by the cutoffs at $x=\pm L_x/2$, $y=\pm L_y/2$, and $z=L_z$. The artificial surface and line contributions introduced by the cutoff at $y=\pm L_y/2$ are proportional to L_xL_z, L_x, and L_z, respectively, and therefore they vanish in the thermodynamic limit $L_y\to\infty$ considered in Eq. (2.2). $\Omega_b(\rho,T,\mu)$ is the bulk free-energy density [see Eq. (A1)], which is minimized by the vapor density $\bar{\rho}_g(T,\mu)$ or the liquid density $\bar{\rho}_l(T,\mu)$. In the following we always take these equilibrium values and therefore we omit the overbars.

The *parallel* surface contribution $\Omega_s^{\parallel}[\rho_+(z),\rho_-(z)]$ has the transparent form

$$\Omega_s^{\parallel}[\rho_+(z),\rho_-(z)]=\tfrac{1}{2}\{\Omega_s^{+}[\rho_+(z)]+\Omega_s^{-}[\rho_-(z)]\}\ , \qquad (2.3)$$

where $\Omega_s^{\pm}[\rho]$ is the surface free-energy density of a liquidlike adsorbed film on a semi-infinite *homogeneous* flat substrate with a substrate potential $V_{\pm}$, respectively

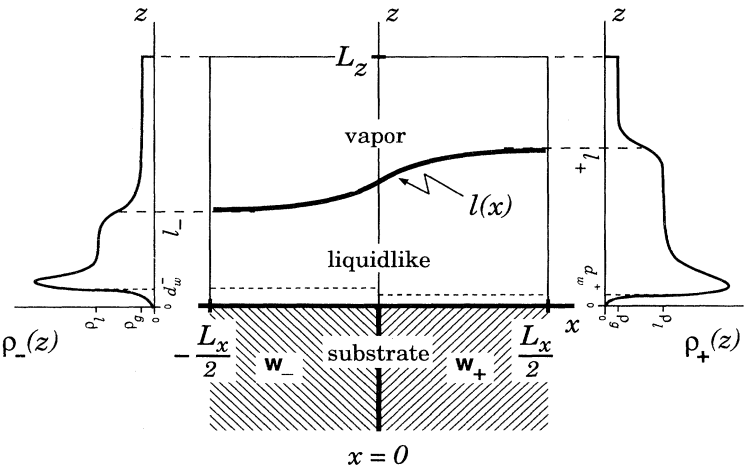

FIG. 2. Schematic density distribution of the fluid exposed to the chemically structured substrate. At large lateral distances $|x|$ from the position $x=0$ of the inhomogeneity the density profile $\rho(x,z)$ reduces to the density profiles $\rho_{\pm}(z)$ of the corresponding homogeneous cases. The profile $l(x)$ of the interface position is defined by $\rho(x,z=l(x))=(\rho_l+\rho_g)/2$. The fluid is enclosed in the box $\Lambda_f=L_x\times L_y\times L_z$ surrounded by vacuum. The repulsive part of the substrate potential leads to the vanishing of $\rho(x,z)$ for $z\to 0$, which can be approximately described by excluded volumes d_w^- and d_w^+. Within our simple choice of a local expression for the reference free energy of the hard-sphere contribution, density oscillations close to the wall are suppressed. Thus our considerations are only reliable if $l(x)$ is large compared to the atomic diameter of the fluid particles.

[see Ref. [4] and Eqs. (A2)–(A9)]. $\bar{\rho}_{\pm}(z)$ minimizes the surface free energy $\Omega_s^{\pm}[\rho(z)]$. Thus solving separately the two homogeneous surface problems renders the asymptotic (i.e., $x=\pm\infty$) equilibrium density profiles $\bar{\rho}_{\pm}(z)$ and determines the wetting characteristics for the two different homogeneous substrate types; note that due to the chemical inhomogeneity of the actual substrate we are concerned with *two* wetting temperatures $T_w^{\pm}$. The *normal* surface contribution $\Omega_s^{\perp}$ is purely artificial [see Eq. (A10)]; it results from cutting off the system at $x=\pm L_x/2$ and thus introducing the fluid-vacuum interfaces.

The equilibrium density configuration $\bar{\rho}(x,z)$ minimizes the line contribution $\Omega_l[\{\rho(x,z)\};\rho_l,\rho_g;T,\mu]$ under the constraint that the quantities ρ_l, ρ_g, and $\rho_{\pm}(z)$ are taken to be those that minimize Ω_b and Ω_s, respectively. The expression for Ω_l consists of an artificial ($\delta\Omega_l[\rho_{\pm}]$) and a physical $\{\Omega_l^{(\mathrm{phys})}[\rho(x,z)]\}$ part:

$$\Omega_l[\rho(x,z)]=\delta\Omega_l[\rho_{\pm}(z)]+\Omega_l^{(\mathrm{phys})}[\rho(x,z)] \ . \tag{2.4}$$

The artificial term, which is induced by the system cutoff, depends only on the asymptotic equilibrium profiles $\rho_{\pm}(z)$ and is constant with respect to the aforementioned constrained minimization of Ω_l since $\rho_{\pm}(z)$ is taken to be $\bar{\rho}_{\pm}(z)$. Therefore the full shape of the density configuration $\rho(x,z)$ is determined only by the physical part of the line contribution. Thus the wetting problem under consideration is associated with the line tension τ of the system, which is given by

$$\tau=\min_{\{\rho\}}(\Omega_l^{(\mathrm{phys})}[\rho])=\Omega_l^{(\mathrm{phys})}[\bar{\rho}(x,z)] \ . \tag{2.5}$$

The explicit expression of the various contributions in Eq. (2.2) are discussed in Appendix A.

The condition for the equilibrium density configuration $\bar{\rho}(x,z)$

$$\left.\frac{\delta\Omega}{\delta\rho}\right|_{\rho=\bar{\rho}(x,z)}\equiv\left.\frac{\delta\Omega_l^{(\mathrm{phys})}}{\delta\rho}\right|_{\rho=\bar{\rho}(x,z)}=0 \tag{2.6}$$

leads to the integral equation

$$0=\mu_{\mathrm{HS}}(\bar{\rho}(x,z),T)-\mu+V(x,z)+\int_{-\infty}^{\infty}dx'\int_{0}^{\infty}dz'\,\bar{w}(|x-x'|,|z-z'|)\bar{\rho}(x',z') \ , \tag{2.7}$$

which has to be solved subject to the boundary conditions $\rho(x\to\pm\infty,z)=\bar{\rho}_{\pm}(z)$. The potential $\bar{w}$ is defined as

$$\bar{w}(x,z)=\int_{-\infty}^{\infty}dy\,\bar{w}((x^2+y^2+z^2)^{1/2})=\bar{w}(x^2+z^2) \tag{2.8}$$

and $\mu_{\mathrm{HS}}(\rho(x,z),T)=\partial f_{\mathrm{HS}}(\rho(x,z),T)/\partial\rho$ denotes the chemical potential of the hard-sphere system. With the bulk quantities and the asymptotic profiles $\bar{\rho}_{\pm}(z)$ fixed, the full solution $\bar{\rho}(x,z)$ of Eq. (2.7) can only be obtained numerically. For that purpose we implement an extended version of the well-established iteration scheme introduced by Tarazona and Evans [39]. The extension compared to flat *homogeneous* geometries involves the additional lateral coordinate x. The convergence criteria of the iteration procedure follow from similar arguments used in the simpler case outlined in Ref. [40].

To solve Eq. (2.7) numerically we truncate $\bar{w}(x^2+z^2)$ at $\Delta=\sqrt{x^2+z^2}=10\sigma$, where σ is the diameter of the fluid particles (see below). As an initial guess for the iterative procedure we use an interpolation between equilibrium profiles $\bar{\rho}(x',z)$ obtained for laterally homogeneous substrate potentials $V(x',z)$ where the fixed values x' are chosen at equal distances over the full lateral range $-L_x'/2<x<L_x'/2$. The combined error in the profiles due to Δ^{-1} and $L_x'^{-1}$ being nonzero is less than 8%. In order to obtain a numerical solution we have to specify the fluid-fluid $[w(r)]$ and the substrate-fluid $[V(x,z)]$ interaction potentials as well as the Helmholtz free-energy density $f_{\mathrm{HS}}(\rho,T)$ of the hard-sphere reference system. For the latter we use the expression due to Carnahan and Starling [41]

$$f_{\mathrm{HS}}(\rho,T)=k_BT\rho\left[\ln(\rho\lambda^3)-1+\frac{4\eta-3\eta^2}{(1-\eta)^2}\right] \tag{2.9}$$

with the thermal de Broglie wavelength λ and the dimensionless packing fraction

$$\eta=\frac{\pi}{6}\rho d^3 \ . \tag{2.10}$$

The hard-sphere diameter d has to be chosen appropriately; see below. For the interparticle pair potential $w(r)$ we take the form

$$w(r)=\epsilon u\left[\frac{r}{\sigma}\right] , \tag{2.11}$$

where

$$u(x)=\begin{cases}4[x^{-12}-x^{-6}] \ , & x<x_0\\ u_0(x^2+1)^{-3} \ , & x>x_0\end{cases} \tag{2.12}$$

with $x_0\simeq 1.2334$ and $u_0\simeq -13.037$. $u(x)$ is continuous and has a continuous derivative at x_0. The motivation for this particular choice for the interparticle potential $w(r)$, which closely resembles the standard Lennard-Jones (LJ) potential for all r, will become apparent below. In the spirit of the WCA procedure [38], we separate $w(r)$ into an attractive part

$$\bar{w}(r)=u_0\frac{\epsilon\sigma^6}{(\sigma^6+r^2)^3} \tag{2.13}$$

for *all* r and into a repulsive part

$$w_{\mathrm{rep}}(r)=[w_{\mathrm{LJ}}(r)+|\bar{w}(r)|]\Theta(x_0\sigma-r) \tag{2.14}$$

so that $w(r)=\bar{w}(r)+w_{\mathrm{rep}}(r)$; $w_{\mathrm{LJ}}(r)=4\epsilon[(\sigma/r)^{12}-(\sigma/r)^6]$. The attractive part with the integrated strength

$$w_0=\int_{\mathbb{R}^3}d^3r\,\bar{w}(|\mathbf{r}|)=u_0\epsilon\sigma^3\frac{\pi^2}{4} \tag{2.15}$$

enters into Eq. (2.1), while the repulsive part leads to the reference free energy as described above [Eqs. (2.9) and (2.10)] with the choice $d=x_0\sigma$. The advantage of this particular choice is that certain integrals involving $\bar{w}(r)$ can be performed analytically. This analytical advantage outweighs the disadvantage that there is a small

difference between our choice of $w(r)$ and the commonly used Lennard-Jones potential and that we slightly modify the standard WCA procedure, which would require $\tilde{w}(r \leq \sigma) = \tilde{w}(r = \sigma)$. The bulk phase diagram that follows from this model is shown in Fig. 3. With this choice one has

$$\tilde{w}(x,z) = w_0 \frac{3\sigma^3}{2\pi} (\sigma^2 + x^2 + z^2)^{-5/2} . \tag{2.16}$$

The substrate potential $V(x,z)$ consists of a short-range repulsive part $V_{\text{rep}}(x,z)$ and a long-range attractive part $V_{\text{att}}(x,z)$:

$$V(x,z) = V_{\text{rep}}(x,z) + V_{\text{att}}(x,z) . \tag{2.17}$$

For the repulsive part of the potential we take the simple form

$$V_{\text{rep}}(x,z) = \Theta(-x) \frac{u_9^-}{z^9} + \Theta(x) \frac{u_9^+}{z^9} . \tag{2.18}$$

The steplike variation of $V_{\text{rep}}(x,z)$ at $x = 0$ in an acceptable approximation because the repulsive part of the pair potentials between the substrate and the fluid particles decays rapidly and because we assume that the transition region between the two substrate halves is sharp. For the attractive part we take

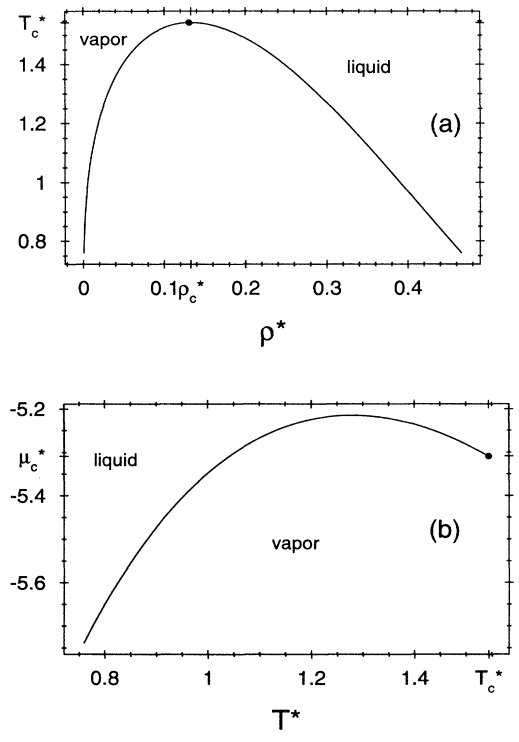

FIG. 3. Bulk phase diagram for the model described in the main text. The liquid-vapor coexistence (a) as function of temperature $T = T^*\epsilon/k_B$ and density $\rho = \rho^*\sigma^{-3}$ and (b) as a function of temperature and chemical potential $\mu = \mu^*\epsilon$. The potential parameters ϵ and σ are defined in Eqs. (2.13) and (2.14).

$$\begin{aligned} V_{\text{att}}(x,z) = & -\frac{u_3^- + u_3^+}{2} \frac{1}{z^3} - \frac{u_3^- - u_3^+}{2} \\ & \times \left\{ \frac{1}{x^3} - \left[\frac{R}{xz} \right]^3 + \frac{3}{2} \frac{1}{Rxz} \right\} - \frac{u_{4,z}^- + u_{4,z}^+}{2} \frac{1}{z^4} \\ & + \frac{u_{4,z}^- - u_{4,z}^+}{2} \left\{ \frac{x}{z^4 R} + \frac{1}{2} \frac{x}{z^2 R^3} \right\} - \frac{u_{4,x}^- - u_{4,x}^+}{2} \\ & \times \left\{ \frac{1}{x^4} - \frac{z}{x^4 R} - \frac{1}{2} \frac{z}{x^2 R^3} \right\} , \quad R = \sqrt{x^2 + z^2} , \end{aligned} \tag{2.19}$$

which follows from summing pair potentials between the fluid particles and the substrate particles located on lattice sites by using the Euler-MacLaurin summation formula [42]. The coefficients $u_3^{\pm}$, $u_{4,x}^{\pm}$, and $u_{4,z}^{\pm}$ can be related to the parameters of these pair potentials including different lateral (x) and orthogonal (z) lattice spacings within both substrates w_+ and w_-. We refrain from presenting these explicit formulas and treat them as free parameters of the substrate potential. The first two terms of $V_{\text{att}}(x,z)$ in Eq. (2.19) are identical to those appearing in Ref. [21]. For large distances z from the substrate and x fixed, $V(x,z)$ vanishes proportional to z^{-3}. For $x \to \pm\infty$, $V(x,z)$ reduces to the substrate potential $V_{\pm}(z)$ of the corresponding semi-infinite, homogeneous, and flat substrate. For $|x| \gg z$ these limiting forms are attained proportional to x^{-3}, so that $V(x,z)$ exhibits the long-range van der Waals character both normal and parallel to the substrate surface. The power law decay of $w(r)$ and $V(x,z)$ induces also various power laws for the shape of the density distribution $\bar{\rho}(x,z)$, which are traditionally called van der Waals tails [4,5]. These aspects will be discussed in Sec. III B.

By carrying out the numerical procedure outlined above we have obtained the equilibrium density distribution $\bar{\rho}(x,z)$ shown in Fig. 4. The thermodynamic state of the system is given by $T_0/T_c = 0.712$ and $\Delta\mu = \mu_0(T_0) - \mu = 1 \times 10^{-5}\epsilon$ so that the bulk of the fluid is in the gas phase with $\rho_g\sigma^3 = 0.0106$. The substrate potential parameters $u_3^{\pm}$ are chosen in such a way that $T_w^+ < T_0 < T_w^-$, where $T_w^+/T_c = 0.648$ and $T_w^-/T_c = 0.842$ with $T_c^* = 1.544$ (see Fig. 3). (This corresponds to the following values of the parameters of the interaction potentials: $u_3^+/t_3 = 0.390$, $u_3^-/t_3 = 0.289$, and $u_{4,x}^{\pm} = u_{4,z}^{\pm} = 20.0\epsilon\sigma^7$.) For critical wetting transitions of the homogeneous semi-infinite substrates $w_{\pm}$ at $T = T_w^{\pm}$ we use the condition $u_3^{\pm} = t_3\rho_l(T = T_w^{\pm})$ (see Ref. [4]), where $\rho_l(T, \mu_0(T))$ is taken to be the liquid density at coexistence, i.e., for $\Delta\mu = 0$. The fluid potential coefficient t_3 is given by Eq. (3.5) (see Sec. III A). For this particular temperature T_0 the bulk liquid density is $\rho_l\sigma^3 = 0.3583$. For these choices within the sharp-kink approximation (cf. Sec. III) the equilibrium film thicknesses $\bar{l}_{\pm}$ for $x \to \pm\infty$ are $\bar{l}_- = 28.44\sigma$ and $\bar{l}_+ = 41.27\sigma$, respectively. These sharp-kink values are estimates for the positions of the actual liquid-vapor interfaces of the asymptotic density distributions $\bar{\rho}_{\pm}(z)$.

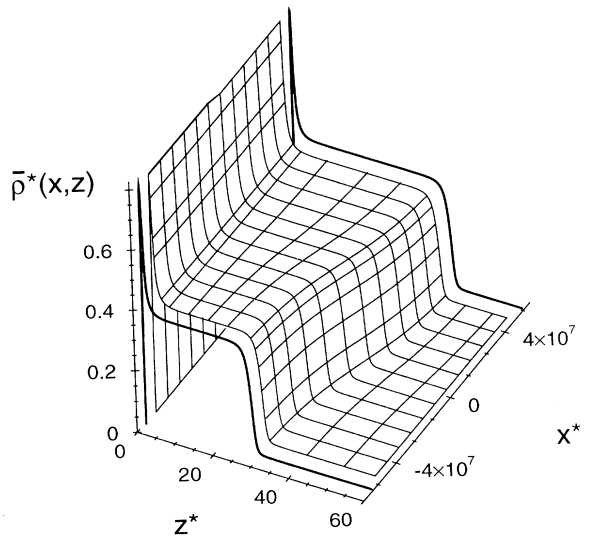

FIG. 4. Equilibrium density distribution $\bar{\rho}^*(x,z)=\bar{\rho}(x,z)\sigma^3$ for $x^*=x/\sigma$ and $z^*=z/\sigma$, respectively. The thermodynamic state of the system and the potential parameters are given in the main text. Note that the scale of the z^* axis is about 1.7×10^6 times larger than the scale of the x^* axis. This means that the transition region in the lateral direction is very large compared to the width of the emerging gas-liquid interface in $\bar{\rho}_\pm(z)=\bar{\rho}(x=\pm\infty,z)$. The asymptotic profiles $\bar{\rho}_\pm(z)$ are shown as bold curves. For $x>0$ ($x<0$), $\bar{\rho}(x,z)$ becomes vanishingly small for $z^*<0.41$ ($z^*<0.42$). The curves correspond to $\bar{\rho}^*(x=\text{const},z)$ and $\bar{\rho}^*(x,z)=\text{const}$, respectively.

$\bar{\rho}(x,z)$ interpolates smoothly between $\bar{\rho}_\pm(z)$. A detailed analysis of the interfacial width of the emerging liquid-vapor interface as inferred from $\bar{\rho}(x,z)$ shows that the variation of the width in the lateral direction due to the bending of the interface is less than 4% of the width of the flat free liquid-vapor interface. This effect is negligible because the curvature of the mean interface position is very small. Therefore, in the present case, the distortion of the actual interface structure as compared with the flat one can be ignored.

III. NONLOCAL INTERFACE HAMILTONIAN

The grand-canonical density functional Ω in Eq. (2.1) is minimized by the equilibrium density distribution $\bar{\rho}(x,z)$ (see, e.g., Fig. 4). Its prominent feature is the position $\bar{l}(x)$ of the emerging liquid-vapor interface. If one is interested only in this aspect it is tempting to determine $\bar{l}(x)$ directly without resorting to the full distribution $\bar{\rho}(x,z)$ and applying the definition $\bar{\rho}(x,z=\bar{l}(x))=(\rho_l+\rho_g)/2$. However, this approach has turned out to be useful only if one is prepared to accept approximations for $\bar{l}(x)$. At low temperatures it is obvious and reasonable to apply the sharp-kink approximation within which the density variation orthogonal to the substrate is taken to be steplike between the bulk values ρ_l and ρ_g. This approximation means that the minimization of Ω is constrained to the subspace of piecewise constant density configurations $\rho(x,z)=\hat{\rho}(x,z)$ with

$$\hat{\rho}[\{l(x)\};x,z;d_w^\pm]=[\Theta(-x)\Theta(z-d_w^-)+\Theta(x)\Theta(z-d_w^+)]\times[\Theta(l(x)-z)\rho_l+\Theta(z-l(x))\rho_g]\,, \tag{3.1}$$

where Θ is the Heaviside function. The first factor in Eq. (3.1) takes into account the excluded volumes $d_w^\pm$ at the wall-liquid interface in a simplified sharp-kink approximation also induced by the repulsive part of the substrate potential [see Eq. (2.18) and Figs. 1 and 2]. The second factor in Eq. (3.1) depends on the mean position $z=l(x)$ of the emerging liquid-vapor interface (see Figs. 1 and 2). By inserting $\hat{\rho}(x,z)$ into the grand-canonical functional Ω given by Eq. (2.1) the latter reduces to a functional of $l(x)$ that depends parametrically also on the fluid-fluid interaction potential $w(r)$ and the substrate potential $V(x,z)$.

For a finite system of size $L_x\times L_y\times L_z$ (see Fig. 5) the systematic decomposition of $\Omega(\{l(x)\})$ within the sharp-kink approximation Eq. (3.1) leads to explicit expressions

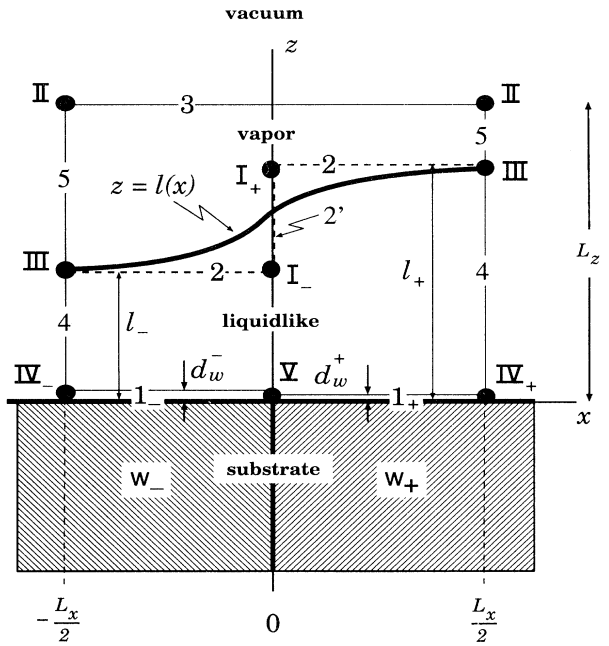

FIG. 5. Illustration of various contributions to surface and line tensions within the sharp-kink approximation for a fluid confined to a finite size $L_x\times L_z$ surrounded by vacuum (compare Figs. 1 and 2). The dashed line corresponds to $l_\infty(x)$ [see Eq. (3.9)]. The planes $x=\pm L_x/2$ and $z=L_z$ define artificial fluid-vacuum interfaces. Surface tensions are denoted by arabic numbers and line tensions by roman numbers: $1_\pm=\sigma_{w_\pm l}$; $3,5=\sigma_{gv}$; $4=\sigma_{lv}$. For $l(x)=l_\infty(x)$ the numbers 2 and 2' correspond to σ_{lg}. The line tensions have the following meaning: $\text{II}=\tau_{gvvv}$, $\text{III}=\tau_{lgvv}$, $\text{IV}_\pm=\tau_{lw_\pm w_\pm v}$, and $\text{V}=\tau_{lw_+w_-l}$, where the indices of τ are self-explanatory abbreviations for the adjacent quarter spaces leading to the corresponding line tension. For $l(x)=l_\infty(x)$ the line tensions $\text{I}_\pm$ are given by $\text{I}_+=\tau_{lggg}$ and $\text{I}_-=\tau_{glll}$. For further explanations and for the explicit forms of the various contributions see the main text and Appendixes A and B.

for the bulk, surface, and line contributions, which are the analogs of those obtained for the general density distribution $\rho(x,z)$ discussed in Appendix A and in Eq. (2.2). The characteristics of the liquid film enter into the surface ($\Omega_s^{\parallel}$) and line (Ω_l) contributions. The latter takes into account the shape of the interface position $l(x)$, whereas the surface free energy depends only on the asymptotic film thicknesses $l_{\pm}=l(x\to\pm\infty)$ (see Appendix B for the explicit expressions and their interpretation). Analogously to the case of the full density theory outlined in Sec. II, the determination of the equilibrium asymptotic boundary values $\bar{l}_{\pm}$ requires the independent minimization of the two surface free energies $\Omega_s^{\pm}(l)$ corresponding to the semi-infinite homogeneous substrates w_+ and w_-, respectively. The determination of the equilibrium film thickness $\bar{l}$ within the sharp-kink approximation for homogeneous substrates is discussed in detail in Ref. [2].

A. Equation for the profile of the interface position

The minimization of $\Omega_l[\{l(x)\}]$, whose explicit form is given in Eqs. (B8) and (B13), with respect to $l(x)$ leads to the following integral equation for the equilibrium profile $\bar{l}(x)$ of the interface position:

$$\Delta\Omega=\Delta\rho[\rho_l t(\bar{l}(x))-V(x,\bar{l}(x))] -(\Delta\rho)^2\int_{-\infty}^{\infty}dx' w^*(x'-x,\bar{l}(x')-\bar{l}(x)) , \quad (3.2)$$

where

$$w^*(x,z)=\int_0^z dz'\bar{w}(x,z') . \quad (3.3)$$

The minimization leading to Eq. (3.2) is carried out under the constraint that the quantities ρ_l,ρ_g,l_+, and l_- take on their equilibrium values. Therefore Eq. (3.2) is supplemented by the boundary conditions $\bar{l}(x\to\pm\infty)=\bar{l}_{\pm}$. Close to two-phase coexistence one has $\Delta\Omega=\Omega_b(\rho_l,T,\mu)-\Omega_b(\rho_g,T,\mu)=\Delta\rho\Delta\mu+O((\Delta\mu)^2)$ with $\Delta\mu=\mu_0(T)-\mu\geq 0$ and $\Delta\rho=\rho_l-\rho_g\geq 0$. The function $t(z)$ corresponds to the interaction energy of a fluid particle located at a distance z from a half space filled by the fluid itself. For the interaction potential $\bar{w}(r)$ defined in Eq. (2.13) one has

$$t(z)=\frac{w_0}{\pi}\left[\frac{\pi}{2}-\arctan(z)-\frac{z}{1+z^2}\right] \quad (3.4)$$

with w_0 defined by Eq. (2.15). For large distances z the asymptotic behavior of $t(z)$ is given by

$$t(z)=-\frac{t_3}{z^3}-\frac{t_4}{z^4}+O(z^{-5}) . \quad (3.5)$$

For $t(z)$ given by Eq. (3.4) one has $t_4=0$ and

$$t_3=-\frac{2}{3}\frac{w_0\sigma^3}{\pi}>0 . \quad (3.6)$$

The kernel in Eq. (3.2) takes on the form

$$w^*(x,z)=\frac{z}{3(x^2+\sigma^2)(x^2+z^2+\sigma^2)^{1/2}} \times\left[\frac{1}{x^2+z^2+\sigma^2}+\frac{2}{x^2+\sigma^2}\right] . \quad (3.7)$$

For thermodynamic paths along the liquid-vapor coexistence curve $\Delta\Omega$ is zero so that in this case the temperature dependence enters only implicitly via the bulk densities $\rho_l(T,\mu_0(T))$ and $\rho_g(T,\mu_0(T))$.

Due to the chemical inhomogeneity the translational symmetry is broken in one lateral direction and gives rise to the explicit dependence of the substrate potential $V(x,z)$ on the coordinate x. The substrate potential enters the equilibrium equation (3.2) only via the difference $\rho_l t(z)-V(x,z)$.

The full solution of Eq. (3.2) can be obtained only numerically, which will be presented in Sec. III C. In the following subsection we discuss analytically the asymptotic behavior of $\bar{l}(x)$ for $|x|\to\infty$.

B. Asymptotic behavior of the profile of the interface position

As already pointed out the separate solutions of the two homogeneous surface problems define the laterally asymptotic structure of the system under consideration. For the following discussion we assume that the potential parameters are chosen in such a way that *critical wetting* transitions occur at T_w^+ and T_w^- on the substrate w_+ and w_-, respectively. In this case, the wetting temperatures $T_w^{\pm}$ are given by the implicit equations (see Ref. [2])

$$u_3^{\pm}=\rho_l(T=T_w^{\pm})t_3 , \quad (3.8)$$

where the potential coefficients $u_3^{\pm}$ and t_3 are defined through Eqs. (2.19) and (3.5), respectively. In the following we assume that $T_w^-<T_w^+$. Since we are concerned with two different substrate types, we focus our attention on the following two situations. First, both substrate types are covered with liquid films of finite thicknesses. Such a situation prevails for any $\mu\leq\mu_0(T)$ with $T<T_w^+$ and off coexistence, i.e., $\mu<\mu_0(T)$, for any T. Second, we consider the situation in which one part of the substrate is *completely* wetted, whereas the thickness of the liquid layer on the other part of the substrate remains finite. For the latter case two possible thermodynamic paths are indicated in the (μ,T)-phase diagram shown in Fig. 6.

In order to examine the first case we consider the bulk system to be *at* coexistence for $T<T_w^+$ and $\mu=\mu_0(T)$ or *off* coexistence for $\mu<\mu_0(T)$ and $T>T_w^{\pm}$ so that *critical wetting* occurs for $T\to T_w^{\pm}$ or *complete wetting* for $\mu\to\mu_0(T)$, respectively.

For convenience we define the steplike interface profile $l_\infty(x)$ as

$$l_\infty(x)=\Theta(-x)l_-+\Theta(x)l_+ . \quad (3.9)$$

Inserting $\bar{l}(x)=l_\infty(x)-\mathrm{sgn}(x)\delta\bar{l}(x)$ with $\delta\bar{l}(|x|\to\infty)=0$ into Eq. (3.2) yields at coexistence, i.e., $\Delta\Omega=0$, the asymptotic behavior of $\bar{l}(x)$ for large values of x:

$$\bar{l}(x\to\pm\infty)=\bar{l}_{\pm}+\frac{\lambda_{3,\mathrm{crit}}^{(\pm)}}{x^3}+O(x^{-4}) \quad (3.10)$$

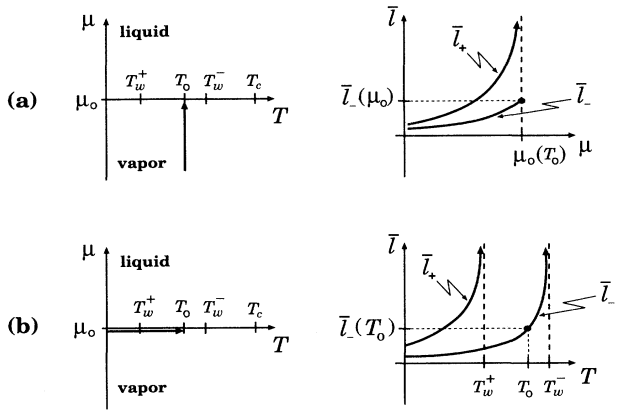

FIG. 6. Various thermodynamic paths in the (μ,T) phase diagram leading to incomplete wetting of the substrate w_- but complete wetting of the substrate w_+ illustrated by the corresponding schematic behavior of the equilibrium film thicknesses $\bar{l}_\pm$. The potential parameters are chosen such that $T_w^+ < T_w^-$. For simplicity the liquid-vapor coexistence curve $\mu_0(T)$ is straightened out (compare Fig. 3). (a) If one approaches $\mu_0(T)$ along an isotherm with $T_w^+ < T_0 < T_w^-$, the substrate w_+ is completely wetted, i.e., $\bar{l}_+ \to +\infty$, whereas the film thickness $\bar{l}_-$ on the substrate w_- remains finite. (b) Upon an increase of the temperature along the liquid-vapor coexistence line the thickness $\bar{l}_+$ of the liquidlike layer on the substrate w_+ diverges at T_w^+ and remains macroscopic for $T_w^+ < T < T_c$; because the temperature T_0 is smaller than T_w^-, the substrate w_- is only incompletely wetted. Both thermodynamic paths lead to the same final state of the system at $(\mu_0(T_0),T_0)$ and thus to the same profile $\bar{l}(x;\mu_0(T_0),T_0)$. This holds also if the wetting transition at T_w^+ is first order, so that in (b) $\bar{l}_+$ would jump to infinity at $T=T_w^+$.

with the amplitude

$$\lambda_{3,\mathrm{crit}}^{(\pm)} = \frac{l_\pm^5}{2} \frac{a_2^- - a_2^+}{(u_4^\pm - t_4\rho_l)\Delta\rho} , \tag{3.11}$$

where we have used the Hamaker constant $a_2^\pm$ for the substrates w_+ and w_-,

$$a_2^\pm = \tfrac{1}{2}\Delta\rho(u_3^\pm - t_3\rho_l) . \tag{3.12}$$

Equation (3.11) applies for a substrate potential of the form given by Eq. (2.19) where we have used the special case $u_{4,x}^\pm = u_{4,z}^\pm \equiv u_4^\pm$. Equation (3.10) holds for sufficiently thick wetting films, i.e., $\bar{l}_\pm \gg d_w^\pm$, and far away from the inhomogeneity, i.e., $|x|/\bar{l}_\pm \gg 1$. *At* coexistence the former requirement is fulfilled if the substrates $w_\pm$ undergo a continuous wetting transition at $T_w^\pm$ so that for $T \to T_w^\pm$ one has $a_2^\pm(T \to T_w^\pm) \to 0-$, which implies [2]

$$\bar{l}_\pm(\Delta\mu = 0^+, T \to T_w^\pm) = \frac{u_4^\pm - (t_4 + 3d_w^\pm t_3)\rho_l(T_w^\pm)}{t_3\rho_l(T) - u_3^\pm} \to \infty . \tag{3.13}$$

[In this case we assume that T_w^+ and T_w^- are close so that even for $T \lesssim T_w^+ < T_w^-$ also $\bar{l}_-(T)$ is already sufficiently large compared with d_w^- (see Fig. 6). Otherwise Eq. (3.10) holds only for $x \to +\infty$.] In the case of critical wetting one has $u_4^\pm - (t_4 + 3d_w^\pm t_3)\rho_l(T) > 0$ so that the denominator in Eq. (3.11) is positive. From Eq. (3.13) it follows that the inequality $\bar{l}_+ > \bar{l}_-$ implies $|a_2^+| < |a_2^-|$ provided $u_4^+ - u_4^- < 3(d_w^+ - d_w^-)t_3\rho_l$. If this is the case one has $\lambda_{3,\mathrm{crit}}^{(\pm)} < 0$ (sine $a_2^\pm < 0$) so that $\bar{l}(x \to +\infty)$ approaches $\bar{l}_+$ from below and $\bar{l}(x \to -\infty)$ approaches $\bar{l}_-$ from above, as depicted in Fig. 5. However, for $u_4^+ - u_4^- > 3(d_w^+ - d_w^-)t_3\rho_l$ the profile $\bar{l}(x \to +\infty)$ approaches $\bar{l}_+$ from above and $\bar{l}(x \to -\infty)$ approaches $\bar{l}_-$ from below.

According to Eq. (3.10), $\bar{l}(x)$ approaches its asymptotic values $\bar{l}_\pm$ as a power law x^{-3}. This behavior is induced by the long-range van der Waals interactions $\sim r^{-6}$ between the fluid particles and between the fluid and substrate particles. Therefore we refer to this part of $\bar{l}(x)$ as the van der Waals tails of the profile of the interface position. [One should recall that there are, in addition, van der Waals details in the density distribution $\bar{\rho}(x,z)$ as a function of z [4,5].]

In the case of *complete wetting*, the asymptotic behavior of $\bar{l}(x)$ is given by a formula similar to Eq. (3.10):

$$\bar{l}(x \to \pm\infty) = \bar{l}_\pm + \frac{\lambda_{3,\mathrm{comp}}^{(\pm)}}{x^3} + O(x^{-4}) \tag{3.14}$$

with

$$\lambda_{3,\mathrm{comp}}^{(\pm)} = \frac{\bar{l}_\pm^4}{6} \frac{a_2^- - a_2^+}{a_2^\pm} . \tag{3.15}$$

As before, Eqs. (3.14) and (3.15) are valid for $|x|/\bar{l}_\pm \gg 1$ and $\bar{l}_\pm \gg d_w^\pm$. The latter is fulfilled if $T > T_w^- > T_w^+$ and $\Delta\mu \to 0+$ so that $\bar{l}_\pm$ with

$$\bar{l}_\pm(\Delta\mu \to 0+, T > T_w^\pm) = \left[\frac{2a_2^\pm}{\Delta\rho\Delta\mu} \right]^{1/3} \tag{3.16}$$

is sufficiently large. For $T_w^- > T > T_w^+$, Eqs (3.14) and (3.15) hold only for $x \to +\infty$. Contrary to the case of critical wetting, the signs of $a_2^- - a_2^+$ and $l_- - l_+$ are definitely linked [see Eq. (3.16)]. (Note that for complete wetting $a_2^\pm$ is positive, but for critical wetting it is negative.) This implies that $\bar{l}(x)$ always approaches its larger asymptotic value from below and its smaller asymptotic value from above. Thus, for complete wetting the profile $\bar{l}(x)$ is monotonic (such as in Fig. 5), whereas in the case of critical wetting a nonmonotonic profile can occur depending on the subdominant terms in the substrate potential. In the limit of a homogeneous substrate one has $\bar{l}_- = \bar{l}_+ = \bar{l}$ and $a_2^- = a_2^+$ so that $\bar{l}(x)$ reduces to $\bar{l}$.

In order to examine the second case mentioned above, i.e., the substrate w_+ is completely wet but w_- is not, we decompose $\bar{l}(x)$ as

$$\bar{l}(x) = \begin{cases} \bar{l}(x) & \text{for } x < \zeta \\ \hat{l}(x) & \text{for } x > \zeta , \end{cases} \tag{3.17}$$

where $x = \zeta \gg \sigma$ denotes the lateral position at which the asymptotic behavior of $\bar{l}(x)$ for large values of x sets in .

For the present purposes we do not have to specify $\tilde{l}(x)$ further.

By inserting Eq. (3.17) into the Euler-Lagrange equation (3.2) we find that for critical wetting $\hat{l}(x)$ behaves like a power law

$$\hat{l}(x)=\alpha_{\kappa}^{\mathrm{crit}} x^{2/(1+\kappa)} , \tag{3.18}$$

where κ is defined via Eq. (B3). For the typical case $\kappa=4$ the profile diverges as $x^{0.4}$. The corresponding amplitude is given by

$$\alpha_4^{\mathrm{crit}}=\left[\frac{25}{2}\frac{a_3^+}{\sigma_{lg}}\right]^{1/5} \tag{3.19}$$

whereas a_3^+ is defined according to Eq. (B3).

In the case of complete wetting the asymptotic behavior of $\hat{l}(x)$ is again given by a power law

$$\hat{l}(x)=\alpha_{\sigma}^{\mathrm{comp}} x^{2/(1+\sigma)} , \tag{3.20}$$

where σ characterizes the asymptotic decay $\sim r^{-(d+\sigma)}$ of the interaction potential between the fluid particles. For van der Waals forces with $\sigma=3$ the profile diverges as the square root (see Refs. [43,44]). For short-range forces, i.e., $\sigma\to\infty$, this growth law turns into a logarithm. The amplitude α_3^{comp} in Eq. (3.20) is given by

$$\alpha_3^{\mathrm{comp}}=\left[8\frac{a_2^+}{\sigma_{lg}}\right]^{1/4} . \tag{3.21}$$

The amplitude α_3^{comp} depends on temperature via the Hamaker constant a_2^+ and the gas-liquid surface tension σ_{lg}. Within the sharp-kink approximation for σ_{lg} [see Eq. (B5)] and by using Eq. (3.12) for the Hamaker constant a_2^+ (which is valid beyond the sharp-kink approximation [4,5]) α_3^{comp} can be expressed analytically in terms of the microscopic interaction potentials; α_3^{comp} depends on both the substrate potential and the fluid-fluid interaction potential. Since one has $a_2^+>0$ for $T>T_w^+$ and $\sigma_{lg}>0$ for $T<T_c$, α_3^{comp} is well defined within the relevant temperature range $T_w^+<T<T_c$ where the power law in Eq. (3.20) holds. If Eq. (3.21) remains valid close to T_c, the amplitude α_3^{comp} will diverge $\sim t^{-(\mu-\beta)/4}$ for $t=(T_c-T)/T_c\to 0$, where β and μ denote the standard bulk critical exponents of the order parameter and the surface tension σ_{lg}, respectively. In the same limit in Eqs. (3.11) and (3.15) $\bar{l}_{\pm}$ must be replaced by the bulk correlation length ξ [4,5] so that $\lambda_{3,\mathrm{crit}}^{(\pm)}\sim\bar{t}_{\pm}^{-5\nu}$ for $\bar{t}_{\pm}=(T_c-T_w^{\pm})/T_c\to 0$ and $\lambda_{3,\mathrm{comp}}^{(\pm)}\sim t^{-4\nu}$ for $t\to 0$, where ν is the bulk critical exponent for the correlation length ξ. All three divergences indicate that close to T_c, the power laws in Eqs. (3.10), (3.14), and (3.20) are replaced by different laws induced by the phenomena of critical adsorption near T_c [5,45–47]. The investigation of critical adsorption on heterogeneous substrates is deferred to future studies.

C. Numerical solution for the profile of the interface position

In the previous two subsections we analyzed the asymptotic properties of the solution corresponding to the nonlocal Euler-Lagrange equation (3.2). However, the *whole* curve $\bar{l}(x)$ is accessible only numerically. Accordingly we have indeed solved Eq. (3.2) numerically by using standard iteration procedures. A typical example of such a solution is shown as the dotted line in Fig. 7. It corresponds to the same thermodynamic state and the same parameters of the interaction potentials as those used in Fig. 4 in which we have displayed the numerical solution of the full integral equation (2.7). This allows us to gauge the quality of the predictions obtained from the effective nonlocal interface Hamiltonian as compared with the full theory. To this end we have extracted from the full density distribution $\bar{\rho}(x,z)$ the interface position corresponding to the definition $\bar{\rho}(x,z=\bar{l}(x))=\frac{1}{2}(\rho_l+\rho_g)$. It is shown as the full line in Fig. 7. The comparison between these two curves shows that the nonlocal effective interface Hamiltonian approximation yields a good account of what one obtains by using the more complicated full theory. The predictions for the interface positions from these two approaches differ by less than 10%. Thus we conclude that the effective interface Hamiltonian provides quantitatively reliable predictions for spatially varying interfaces. As will be shown later this is not true for the *local* version of the effective interface Hamiltonian (cf. Sec. IV).

IV. LOCAL INTERFACE HAMILTONIAN

The analysis in the preceding section is based on the *nonlocal* integral equation (3.2). By applying a gradient expansion for the nonlocal term (see Refs. [49–51]) Eq. (3.2) can be approximated by a *local,* nonlinear

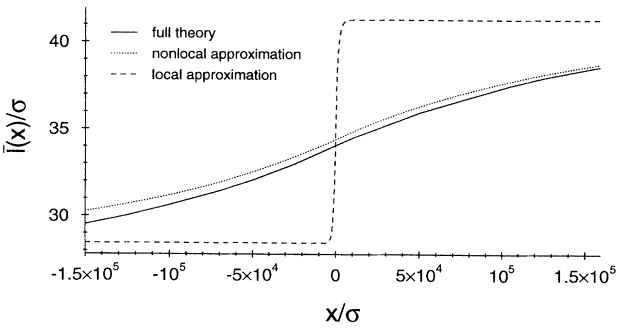

FIG. 7. Profiles of the interface position $\bar{l}(x)$ for the same system obtained by three different methods. The full curve follows from the density distribution $\bar{\rho}(x,z)$ according to the definition $\bar{\rho}(x,z)=(\bar{\rho}_l+\bar{\rho}_g)/2$ by solving Eq. (2.7) numerically. The dotted curve corresponds to the nonlocal interface Hamiltonian [Eq. (3.2)], whereas the dashed curve is obtained from the local interface Hamiltonian [Eq. (4.1)]. The thermodynamic state of the fluid and the potential parameters that have been used are described in the main text. Whereas the nonlocal interface Hamiltonian describes the actual profile rather well, the local Hamiltonian exaggerates the variation near the inhomogeneity drastically. Since the scale of the ordinate is about 10^4 times larger than that of the abscissa, the profile is very broad. Thus close to liquid-vapor coexistence the sharp chemical inhomogeneity of the substrate does not succeed in maintaining a sharp variation of the density of the adsorbed liquidlike film.

differential equation for the equilibrium profile $\overline{l}(x)$ of the interface position:

$$\Delta\Omega-\Delta\rho U(x,\overline{l}(x))=\sigma_{lg}\frac{d^2\overline{l}(x)}{dx^2}\left[1+\left[\frac{d\overline{l}(x)}{dx}\right]^2\right]^{-3/2} +(\text{higher-order terms}) \quad (4.1)$$

with

$$U(x,z)=\rho_l t(z)-V(x,z) . \quad (4.2)$$

Starting from Eq. (3.2) it turns out that in Eq. (4.1), σ_{lg} is given by the sharp-kink approximation for the surface tension of the flat liquid-vapor interface [see Eq. (B5)]. The higher-order terms in Eq. (4.1) contain at least the square of $d^2\overline{l}(x)/dx^2$ or third-order derivatives of $\overline{l}(x)$. The leading term on the right-hand side of Eq. (4.1) recalls the construction scheme of phenomenological approaches [52]. There the cost $\Delta\mathcal{F}$ in free energy due to the distortion $F(\mathbf{R}=(x,y))$ of a flat interface is taken to be the surface tension σ_{lg} of this flat interface times the corresponding increase of interfacial area with respect to a flat reference plane A defined by $F(\mathbf{R})=$const:

$$\Delta\mathcal{F}=\sigma_{lg}\int_A d^2R\{\sqrt{1+[\nabla F(\mathbf{R})]^2}-1\} . \quad (4.3)$$

The functional derivative of Eq. (4.3) with respect to $F(\mathbf{R})$ yields the right-hand side of Eq. (4.1) for a mean profile that is independent of y. Although Eq. (4.3) is frequently used for a variety of problems, one has to keep in mind that this expression is justified microscopically only for such, rather artificial, interaction potentials between the fluid particles that are exactly zero outside a certain range. For exponentially decaying forces the sum of the higher-order terms in Eq. (4.1) diverges and for realistic van der Waals potentials the coefficients of the individual higher-order terms are infinite (see Refs. [49–51]). Therefore, at best, Eq. (4.1) can be viewed as corresponding to an effective theory that, however, may fail both qualitatively and quantitatively. It is the purpose of this section to check the reliability of the local interface Hamiltonian. This is desirable because the local version is significantly easier to handle both analytically and numerically so that one would like to know for which aspects the more difficult nonlocal version is indispensable.

First, we considered the van der Waals tails of $\overline{l}(x)$ for $|x|\to\infty$ in the case of complete and critical wetting if $\overline{l}_\pm<\infty$ and the power law of $\overline{l}(x\to+\infty)$ if $\overline{l}_+=\infty$. It turns out that the corresponding results obtained for the nonlocal theory in Sec. III B [Eqs. (3.10), (3.11), (3.14), (3.15), (3.20), and (3.21)] remain valid even for the local theory in Eq. (4.1). This means that the local theory predicts both the power laws of these particular van der Waals tails and the analytical expressions for their amplitudes correctly. To a certain extent this result is surprising and could not be anticipated because in a similar situation of a liquid film adsorbed on a wedgelike substrate the amplitudes of the van der Waals tails appearing there are predicted incorrectly by the local theory [19]. A close examination of the nonlocal interface Hamiltonian shows that this difference with respect to the local approximation can be traced back to the fact that in the wedge geometry $\overline{l}(x)$ is forced to diverge linearly for $|x|\to\infty$, whereas in the present case of a chemically structured substrate $\overline{l}(x)$ diverges weakly [see Eq. (3.20)].

Second, we analyze the behavior of $\overline{l}(x)$ around $x=0$ where it varies most. To this end Eq. (4.1) must be solved numerically for given bulk and surface parameters and for the boundary conditions $\overline{l}(x\to\pm\infty)=\overline{l}_\pm$. In order to solve this boundary value problem, we have used a self-adjusting algorithm that implements a shooting and matching scheme in order to overcome numerical and conceptional insufficiencies of library routines. The solution of Eq. (4.1) is obtained by guessing an initial slope of $\overline{l}(x)$ at $x=-L_x/2$, say, $\overline{l}'_-$. Using a standard fourth-order Runge-Kutta routine with initial values $\overline{l}(x=-L_x/2)=\overline{l}_-$ and $\overline{l}'(x=-L_x/2)=\overline{l}'_-$, the solution at $x=L_x/2$ is compared with the desired value $\overline{l}(x=L_x/2)=\overline{l}_+$. An appropriate readjustment of $\overline{l}'(x=-L_x/2)$ is performed automatically until $|\overline{l}(x=L_x/2)-\overline{l}_+|<\Delta_+$ where Δ_+ is a prescribed accuracy. In the particular case that the substrate w_+ is completely wet but w_- remains nonwet, the boundary condition at $x=L_x/2$ with $L_x/\sigma\gg1$ is replaced by $\overline{l}(x=L_x/2)=\alpha_3\sqrt{L_x/2}$. Thus the knowledge of the analytical result in Eqs. (3.20) and (3.21) is indispensable for the numerical solution of Eq. (4.1) [53].

Figure 8(a) displays the numerical solutions $\overline{l}(x)$ along the isotherm $T_0/T_c=0.712$ for $\Delta\mu\to0$. (The temperature and the parameters of the interaction potentials are again those used in Fig. 4.) This isotherm leads to complete wetting of the substrate w_+ but incomplete wetting of the substrate w_- in the limit $\Delta\mu^*=[\mu_0(T)-\mu]/\epsilon\to0+$; it corresponds to $\rho_l\sigma^3=0.3583$. The transition region around $x=0$ can be described by the position of the turning point x_{TP} and the locations x_0^+ and x_0^- at which $\overline{l}(x)$ deviates by 20% from the asymptotic values $\overline{l}_-$ on the left-hand side and $\overline{l}_+$ on the right-hand side, respectively. Whereas x_{TP} and x_0^- remain finite in the limit $\Delta\mu\to0$, x_0^+ diverges like $(\Delta\mu)^{-2/3}$. This broadening of the lateral structure is clearly visible in Fig. 8(b). The power law divergence of x_0^+, which follows from the numerical solution of Eq. (4.1) for the interparticle potential $\tilde{w}(r)$ given by Eq. (2.13), can be also checked analytically by approximating $\overline{l}(x)$ according to the prescription given in Eqs. (3.16), (5.5), and (5.6).

It has been proposed [48] that the singular behavior of the line tension at T_w is similar to the corresponding behavior of the surface tension at critical end points. If this analogy is extended also to *local* properties one is lead to the following scaling prediction for the profile $\overline{l}(x)$:

$$\overline{l}(x)=\overline{l}_+f(x/\xi_\perp) \quad (4.4)$$

with $\xi_\perp\sim(\overline{l}_+)^{(\sigma+1)/2}$, which are valid for x and $\overline{l}_+$ sufficiently large [54]. The scaling function $f(y)$ must have the analytic properties $f(\infty)=1$ and $f(y\to0)\sim y^{2/(\sigma+1)}$. Equation (4.4) has a structure similar to the order parameter profile for critical adsorption at a plane wall. There it has been shown that the corresponding scaling function is universal in the sense of the renormalization group theory [45–47]. Whether this is

also true for the scaling function in Eq. (4.4) remains to be seen. Equation (4.4) is expected to hold also for critical wetting with σ replaced by κ [see Eq. (3.18)] and with $\bar{l}_+$ replaced by Eq. (3.13) with $\bar{l}_+ \sim (T_w^+ - T)^{-1}$ so that in this case x_0^+ diverges like $(T_w^+ - T)^{-2}$. The scaling function $f(y)$ will be different for critical and complete wetting, but both have the same analytic properties for $y \to 0$ and $y \to \infty$.

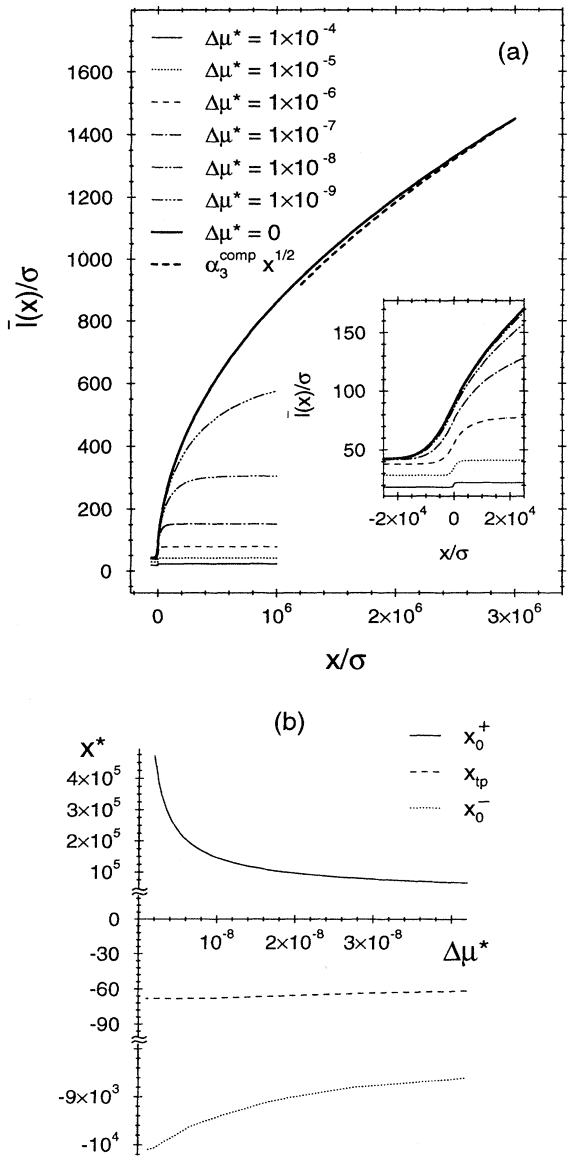

FIG. 8. (a) Profile $\bar{l}(x)$ of the interface position as predicted by Eq. (4.1) for an isotherm at $T_0/T_c = 0.712$ and complete wetting $\Delta\mu^* = \Delta\mu/\epsilon \to 0+$. The substrate w_+ at $x \geq 0$ is wetted completely whereas the substrate w_- remains only partially wet. The parameters of the interaction potentials are given in the main text. At coexistence, $\Delta\mu = 0+$, the profile diverges as $\alpha_3^{\rm comp} x^{1/2}$, as predicted analytically (thick dashed curve). (b) Positions of the turning point $x_{\rm TP}$ and the locations x_0^+ and x_0^- at which $\bar{l}(x)$ deviates by 20% from the asymptotic values $\bar{l}_-$ on the left-hand side and $\bar{l}_+$ on the right-hand side, respectively, for $\Delta\mu \to 0$. x_0^+ diverges as $\Delta\mu^{-2/3}$ and leads to a clearly visible broadening of the profile around $x = 0$ for $\Delta\mu \to 0$. $x_{\rm TP}$ and x_0^- attain finite values for $\Delta\mu \to 0$. Note that the scale of the ordinate in (a) is 2700 times larger than the scale of abscissa.

After having discussed the analytic properties of the local approximation of $\bar{l}(x)$ we now analyze the *quantitative* reliability of this approximation. To this end we compare the interface position predicted by the local approximation with those obtained from the nonlocal approximation and from the full theory, respectively. As the dashed line in Fig. 7 shows, the local approximation for $\bar{l}(x)$ fails quantitatively, although all three curves have the *same* asymptotic behavior for $|x| \to \infty$. The local approximation underestimates the width of the interfacial structure around $x = 0$ and exaggerates its variation at $x = 0$ drastically. Therefore we conclude that the nonlocal effective interface Hamiltonian yields reliable predictions whereas the local approximation fails significantly; under favorable circumstances the local approximation allows one to extract the correct asymptotic behavior of interface profiles (see the second paragraph in this section), but it is not reliable qualitatively.

V. LINE TENSION

According to Eq. (2.5) the equilibrium density distribution $\bar{\rho}(x,z)$ minimizes the line contribution $\Omega_l^{(\rm phys)}$ to the grand-canonical free-energy functional and yields the line tension τ of the fluid associated with the lateral inhomogeneity. Since the full expression for $\Omega_l^{(\rm phys)}$ [see Eqs. (A19)–(A25)] contains a quadrupole integral and therefore is rather difficult to analyze either analytically or numerically, we resort to the effective description in terms of the profile $\bar{l}(x)$ for the interface position. Within this description $\Omega_l^{(\rm phys)}$ is replaced by $\Delta\omega[\bar{l}(x)]$ [see Eq. (B11)], which is now reduced to a double integral [see Eq. (B12)] and can be analyzed numerically (cf. Sec. V C). In view of the minor discrepancy between the predictions of the full density distribution $\bar{\rho}(x,z)$ and the nonlocal interface Hamiltonian (see Fig. 8) the values of τ obtained from this approach are expected to be quantitatively useful. In Sec. IV we showed how the nonlocal effective interface Hamiltonian can be further approximated by a local expression. Although this leads to a significant deterioration of the quantitative reliability, it turned out that this local approximation nonetheless captures all asymptotic features of the profile $\bar{l}(x)$ correctly. Therefore we expect that the leading singular behavior of τ close to the wetting transition can be inferred reliably from the expression for the line contribution within the local approximation. This analysis is facilitated by the fact that in the local approximation τ is reduced to a single integral.

By applying the systematic gradient expansion, which is described in Refs. [49–51] and leads from Eq. (3.2) to (4.1), one obtains, from the nonlocal expressions in Appendix B, the following functional for the physical line contribution corresponding to the local effective interface Hamiltonian:

$$\tau_{\rm loc}=\int_{-\infty}^{\infty}dx\left[\sigma_{lg}\left\{\left[1+\left[\frac{dl}{dx}\right]^2\right]^{1/2}-1\right\}+\Delta\phi(x,l(x))\right]+\omega_l(\bar{l}_+,\bar{l}_-)\ , \tag{5.1}$$

where the constant $\omega_l(\bar{l}_+,\bar{l}_-)$ is given by Eq. (B12) in Appendix B. The function $\Delta\phi$ is defined as

$$\Delta\phi(x,l(x))=\phi(x,l(x))-\phi(x,\bar{l}_\infty(x))\ , \tag{5.2}$$

where $\bar{l}_\infty(x)=\Theta(-x)\bar{l}_-+\Theta(x)\bar{l}_+$ and

$$\phi(x,z)=\Delta\Omega z-\frac{\Delta\rho}{2}\left[t_3\rho_l-\frac{u_3^+ +u_3^-}{2}\right]\frac{1}{[z-d_w^\infty(x)]^2}+\Delta\rho\frac{u_3^+ -u_3^-}{2}\left[\frac{z-d_w^\infty(x)-r}{x^3}+\frac{r}{4x[z-d_w^\infty(x)]^2}\right] \tag{5.3}$$

with $r=\sqrt{x^2+[z-d_w^\infty(x)]^2}$ and $d_w^\infty(x)$ given by Eq. (B18). For wetting transitions along the liquid-vapor coexistence line, one has $\Delta\Omega=0$; in this case the whole temperature dependence enters implicitly via the bulk densities ρ_l and ρ_g. The functional derivative of $\tau_{\rm loc}$ renders Eq. (4.1), whose solution $\bar{l}(x)$ yields the line tension $\bar{\tau}_{\rm loc}=\tau_{\rm loc}[\{l(x)=\bar{l}(x)\},l_\pm=\bar{l}_\pm]$. One should realize that Eq. (5.1) is free from any arbitrariness that comes into play if one starts from a phenomenological ansatz for τ. In the limit $\bar{l}(x)\to\infty$, $\bar{\tau}_{\rm loc}$reduces to the line tension of a semi-infinite liquid exposed to an inhomogeneous substrate:

$$\bar{\tau}_{\rm loc}[\{\bar{l}(x)\to\infty\},\bar{l}_+,\bar{l}_-]=\tau_{lw_+w_-l} \tag{5.4}$$

with $\tau_{lw_+w_-l}$ given by Eq. (B20).

Finally, we want to emphasize that the above line tension τ is defined for *all* values of μ and T. Previous calculations of other line tensions are tied either to liquid-vapor coexistence $\mu=\mu_0(T)$ for the line tension associated with the contact line of liquid, vapor, and a substrate [48] or to the prewetting line, which allows one to study the coexistence of thin and thick films on a *homogeneous* substrate [36]. (For a review see Ref. [54].) In both cases the translational invariance in the lateral direction is broken by boundary conditions at $x=\pm\infty$, whereas in our case it is broken by the inhomogeneity of the substrate. [Technically the treatment of a chemically inhomogeneous substrate is more difficult because the lateral variation of the substrate potential acts like a time-dependent external potential in the mechanical analog of a one-dimensional motion of a particle with coordinate l and time variable x described by Eq. (4.1). This precludes the exploitation of the energy conservation law, which is possible in other cases.]

Since the asymptotic behavior of the profile of the interface position is predicted correctly by the local interface Hamiltonian (see Sec. IV), we assume that it yields reliably the leading singular behavior of the line tension τ in the limit $\Delta\mu\to0$ for $T_w^+<T<T_w^-$, in which case the substrate w_+ is wetted and w_- not, and in the limit $T\to T_w^+$ at coexistence $\Delta\mu=0^+$ corresponding to critical wetting. To this end we introduce the trial function

$$\tilde{l}(x)=\begin{cases}\bar{l}_-(x) & \text{for } x<\mathcal{L}\\ \bar{l}_+(x) & \text{for } x>\mathcal{L}\ .\end{cases} \tag{5.5}$$

Here $x=\mathcal{L}\gg\sigma$ denotes the position where the two trial functions $\bar{l}_-(x)$ and $\bar{l}_+(x)$ intersect. For temperatures T above the wetting temperature T_w^+ the crossover from a finite to an infinite film thickness $\bar{l}_+$ is induced by $\Delta\mu\to0$, whereas below T_w^+ it is induced at coexistence for $T\to T_w^+$. In the case of complete wetting and for large positive values of $x>\mathcal{L}$ the corresponding behavior of the interfacial profile $\tilde{l}_+(x)$ is taken as

$$\tilde{l}_+(x)=\bar{l}_+\left\{\frac{y^6}{q_{\rm comp}+y^6}+\frac{y}{1+y^7}\right\} \tag{5.6}$$

with $y=\alpha_3^{\rm comp}\sqrt{x}\,/\bar{l}_+$. The above formula interpolates smoothly between the previously derived asymptotic behaviors of $\tilde{l}_+(x)$:

$$\tilde{l}_+(x)=\begin{cases}\alpha_3^{\rm comp}\sqrt{x} & \text{for } \bar{l}_+=\infty\ ,\ x<\infty\\ \bar{l}_+ +\dfrac{\bar{l}_+^{\,7}(1-q_{\rm comp})}{(\alpha_3^{\rm comp})^6}x^{-3} & \text{for } x\to\infty\ ,\ \bar{l}_+<\infty\ .\end{cases} \tag{5.7}$$

The comparison with Eqs. (3.11), (3.15), and (3.21) yields the constant $q_{\rm comp}$,

$$q_{\rm comp}=1+\frac{1}{6}\left[1-\frac{a_2^-}{a_2^+}\right]\left[\frac{8a_2^+}{\sigma_{lg}}\frac{1}{\bar{l}_+^2}\right]^{3/2}\ . \tag{5.8}$$

Thus the expression in Eq. (5.6) takes into account both the van der Waals tails of the profile and its square root divergence at coexistence. Since we chose $T<T_w^-$, the film thickness $\bar{l}_-$ remains finite; therefore $\tilde{l}_-(x)$ is a bounded function for $x<\mathcal{L}$.

According to the discussion given above, the leading singular behavior of the line tension $\bar{\tau}$ follows upon inserting Eq. (5.5) into Eq. (5.1). Since the singularity of $\bar{\tau}$ is induced by the unlimited growth of $\bar{l}_+$ one finds

$$\bar{\tau}_{\rm sing}=\int_{\mathcal{L}}^{\infty}dx\left[\sigma_{lg}\left\{\left[1+\left[\frac{d\bar{l}_+}{dx}\right]^2\right]^{1/2}-1\right\}+\Delta\phi(x,\bar{l}_+(x))\right]\ . \tag{5.9}$$

The contributions due to $\bar{l}_-(x)$ and $\omega_l(\bar{l}_+,\bar{l}_-)$ remain finite for $\bar{l}_+\to\infty$. Since $|d\bar{l}_+/dx|\ll1$, the gradient term in Eq. (5.9) can be expanded and leads to a contribution $\frac{1}{4}\sigma_{lg}(\alpha_3^{\rm comp})^2\ln(\bar{l}_+/\sigma)$ up to terms constant in $\bar{l}_+$. The second term in Eq. (5.9) yields $a_2^+\,(\alpha_3^{\rm comp})^{-2}\ln(\bar{l}_+/\sigma)+(a_2^+-a_2^-)\bar{l}_+^{-3}(\alpha_3^{\rm comp})^4\ln(\bar{l}_+/\sigma)$ up to terms constant in $\bar{l}_+$. It turns out that all three contributions are independent of the parameter $q_{\rm comp}$ entering Eq. (5.6), which describes the lateral van der Waals tails. By using

the expression for $\alpha_3^{\rm comp}$ [Eq. (3.21)] we finally arrive at

$$\bar{\tau}_{\rm sing}^{\rm comp}=\frac{3\sqrt{2}}{4}\sqrt{a_2^+\sigma_{lg}}\ln\left[\frac{\bar{l}_+}{\sigma}\right]+8\frac{a_2^+(a_2^+-a_2^-)}{\sigma_{lg}}\frac{1}{\bar{l}_+^3}\ln\left[\frac{\bar{l}_+}{\sigma}\right]+\text{const}\ . \tag{5.10}$$

Note that, as it should, $\bar{\tau}_{\rm sing}$ is independent of the unspecified intersection point $\mathcal{L}$ introduced in Eq. (5.5). For complete wetting Eq. (5.10) leads to [see Eq. (3.16)]

$$\bar{\tau}_{\rm sing}^{\rm comp}(\Delta\mu\to 0)=-\frac{\sqrt{2}}{4}\sqrt{a_2^+\sigma_{lg}}\ln\left[\frac{\Delta\mu}{2a_2^+/(\sigma^3\Delta\rho)}\right]-\frac{4}{3}\frac{\Delta\rho(a_2^+-a_2^-)}{\sigma_{lg}}\times\Delta\mu\ln\left[\frac{\Delta\mu}{2a_2^+/(\sigma^3\Delta\rho)}\right]+\text{const}\ . \tag{5.11}$$

In leading order $\bar{\tau}_{\rm sing}^{\rm comp}$ is proportional to the square root of the Hamaker constant a_2^+ of the completely wetted substrate and the surface tension σ_{lg} of the liquid-vapor interface. The same type of divergence of the line tension is found when approaching a first-order wetting transition along the prewetting line [36].

In the case of critical wetting the same analysis can be applied. For large positive values of $x>\mathcal{L}$ the interfacial profile $\tilde{l}_+(x)$ is taken as

$$\tilde{l}_+(x)=\bar{l}_+\left\{\frac{y^{15/2}}{q_{\rm crit}+y^{15/2}}+\frac{y}{1+y^{11}}\right\} \tag{5.12}$$

with $y=\alpha_4^{\rm crit}x^{2/5}/\bar{l}_+$. Analogously to the case of complete wetting [see Eq. (5.7)], the asymptotic behavior of the interfacial profile $\tilde{l}(x)$ in the case of critical wetting is captured correctly by Eq. (5.12) for both finite and infinite $\bar{l}_+$ [see Eqs. (3.10) and (3.19), respectively]. Using Eqs. (3.10), (3.11), and (3.19) the constant $q_{\rm crit}$ is given by

$$q_{\rm crit}=\frac{1}{2}\frac{a_2^+-a_2^-}{\sigma_{lg}\bar{l}_+^2}\left[\frac{u_{4,z}^+\Delta\rho}{\sigma_{lg}\bar{l}_+^3}\right]^{1/2}. \tag{5.13}$$

Upon inserting Eqs. (5.5), (5.12), and (5.13) into Eq. (5.1) one obtains the following expression for the leading singularity of the line tension:

$$\bar{\tau}_{\rm sing}^{\rm crit}(T\to T_w^+)=\tfrac{3}{4}a_2^-(T_w^+)[\ln(\bar{l}_+/\sigma)]/\bar{l}_++\text{const}\ , \tag{5.14}$$

where $\bar{l}_+$ is given by Eq. (3.13) and $a_2^-(T_w^+)<0$. Expressed in terms of the reduced temperature $\delta=(T-T_w^+)/T_w^+<0$ one has [see Eq. (3.12)] $a_2^+(T)=\alpha\delta+\cdots,\ \alpha>0$,

$$\bar{\tau}_{\rm sing}^{\rm crit}(\delta\to 0-)=-\frac{1}{2\alpha}|a_2^-(T_w^+)|a_3^+(T_w^+)|\delta|\ln\frac{1}{|\delta|}+\text{const}\ , \tag{5.15}$$

where $a_3^+(T_w^+)$ is positive. This shows that, as in the case of complete wetting, the line tension reaches a maximum at the wetting transition. However, in contrast to complete wetting, in the case of critical wetting the line tension remains finite and reaches its maximum via a cusplike singularity.

The above analytic expressions for the line tension are valid asymptotically in the limit $\bar{l}_+\to\infty$ and capture only its leading singular behavior. The determination of the full line tension $\bar{\tau}$ requires one to evaluate Eq. (5.1) numerically. For the same set of parameters that have been used for Fig. 7, the result for complete wetting is shown in Fig. 9. As illustrated by the inset the leading asymptotic behavior $\bar{\tau}\sim|\ln\Delta\mu^*|$ is confined only to the narrow region $\Delta\mu^*\lesssim 1\times10^{-10}$. Thus we conclude that for experimentally accessible values for the undersaturation the full expression in Eq. (5.1) must be used.

Figure 9 shows that the typical order of magnitude of the line tension associated with the chemical inhomogeneity considered here is $\bar{\tau}\simeq\epsilon/\sigma$. Taking interaction potential parameters for argon ($\epsilon=122k_BK$, $\sigma=3.4$ Å) or for *n*-heptane ($\epsilon=573k_BK$, $\sigma=6.25$ Å) [55], this leads to an estimate of $\bar{\tau}\simeq10^{-11}$ N. Compared with the experimental values 10^{-5}–10^{-6} N [56–58] for the line tension of three fluid phase contact lines, the line tension due to the chemical inhomogeneity is drastically smaller. Future studies, which should also take into account the gravitational field, have to reveal whether this large difference is caused by either the particular type of spatial

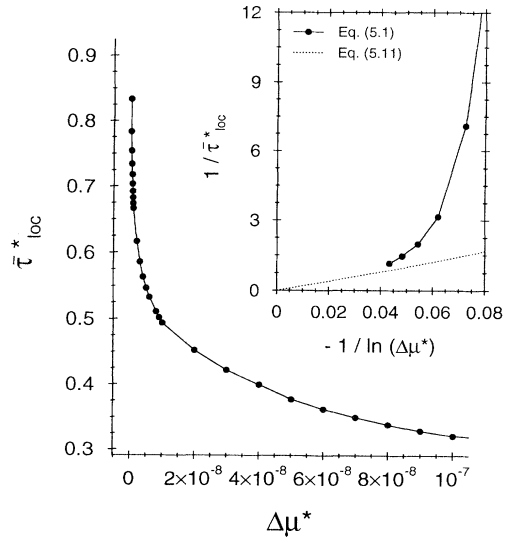

FIG. 9. Line tension $\bar{\tau}^*_{\rm loc}=\bar{\tau}_{\rm loc}\sigma/\epsilon$ in the local approximation [Eq. (5.1)] diverges logarithmically for complete wetting $\Delta\mu\to0$. As illustrated in the inset, the leading singular behavior for $\Delta\mu\to0$ [first term in Eq. (5.11)] is confined to under-saturations $\Delta\mu^*\lesssim1\times10^{-10}$. The parameters used here are the same as for Fig. 7.

inhomogeneity considered here or the use of the local approximation, or both.

The nonlocal expression for the line tension τ in the system is given by [see Eqs. (B8) and (B11)]

$$\bar{\tau}=\Delta\omega[\bar{l}(x)] \ . \tag{5.16}$$

In view of Fig. 9 we expect that $\bar{\tau}_{\text{nonloc}}$ yields a quantitatively reliable estimate for the actual line tension $\bar{\tau}$ based on the full distribution $\bar{\rho}(x,z)$ [see Eqs. (A18)–(A25)]. The calculation of the actual line tension $\bar{\tau}$ is a demanding numerical task involving quadruple integrals, which we leave to future studies.

VI. SUMMARY

We have obtained the following results.

(i) We have formulated a microscopic description of a simple fluid with long-range forces exposed to a chemically inhomogeneous substrate (Sec. II). A systematic decomposition of the grand-canonical density-functional yields explicit expressions for bulk, surface, and line contributions [Eqs. (2.2), (A1), (A2), (A10), and (A11)].

(ii) The equilibrium number density distribution $\bar{\rho}(x,z)$ minimizes the line contribution to the free energy. It is determined by a nonlinear integral equation [Eq. (2.7)], which is solved numerally (Fig. 4).

(iii) The lateral variation of the density distribution is approximated reasonably well by a nonlocal effective interface Hamiltonian [Eqs. (3.2) and (B8)]. The corresponding numerical results are shown in Fig. 7.

(iv) If the substrate is not wet, the film thickness attains its asymptotic values in lateral directions via van der Waals details whose power laws and prefactors have been determined analytically both for complete and critical wetting [Eqs. (3.10), (3.11), (3.14), and (3.15)].

(v) If one of the substrates is wet the film thickness diverges as function of the lateral coordinate x as a power law whose amplitude is also known analytically [Eqs. (3.20) and (3.21)]. For $T>T_w^+$ and at T_w^+ of first-order wetting this thickness diverges as $x^{1/2}$ for nonretarded dispersion forces, whereas at T_w^+ of a second-order wetting transition it diverges as $x^{2/5}$.

(vi) Close to wetting transitions the interface profile broadens and exhibits a scaling behavior [Eq. (4.4) and Fig. 8].

(vii) The frequently used local effective interface Hamiltonian exaggerates the variation of the interface profile drastically. Although in this particular case it predicts the asymptotic behavior correctly, it fails quantitatively (Fig. 7).

(viii) For van der Waals forces the line tension of the system diverges logarithmically for complete wetting [Eq. (5.11) and Fig. 9]. For critical wetting the line tension attains a finite maximum via a cusplike singularity [Eqs. (5.14) and (5.15)].

ACKNOWLEDGMENT

One of the authors (M.N.) acknowledges the support by Grant No. KBN27029101 of the Committee for Scientific Research in Poland.

APPENDIX A: DEPENDENCE OF THE DENSITY FUNCTIONAL ON THE SYSTEM SIZE

In order to separate the grand-canonical functional in Eq. (2.1) into its bulk, surface, and line contributions [see Eq. (2.2)] we consider a fluid that is confined to a finite volume $\Lambda_f=\{\mathbf{r}\in\mathbb{R}^3|-L_x/2<x<L_x/2, \ -L_y/2<y<L_y/2, \ 0<z<L_z\}$. The planes $x=\pm L_x/2$, $y=\pm L_y/2$, and $z=L_z$ define artificial fluid-vacuum interfaces (see Fig. 2).

The bulk contribution Ω_b is given by the bulk free-energy density of the vapor phase,

$$\Omega_b^{(g)}(\rho_g,T,\mu)=f_{\text{HS}}(\rho_g,T)+\tfrac{1}{2}w_0\rho_g^2-\mu\rho_g \tag{A1}$$

for the definition of w_0 see Eq. (2.15). The surface contribution $\Omega_s^{\parallel}[\{\rho\}]$ consists of two terms, each describing the surface free-energy density of a fluid in the presence of a homogeneous semi-infinite substrate:

$$\Omega_s^{\parallel}[\rho_+(z),\rho_-(z)]=\tfrac{1}{2}\{\Omega_s^+[\rho_+(z)]+\Omega_s^-[\rho_-(z)]\} \tag{A2}$$

with (see Ref. [4])

$$\begin{aligned}\Omega_s^{\pm}[\{\rho_\pm(z)\};\rho_l,\rho_g,T,\mu]=&\int_0^\infty dz\,\Delta f_{\text{HS}}(\rho_\pm(z),T)-\mu\int_0^\infty dz\,\delta\rho_\pm(z)+\int_0^\infty dz\,V_\pm(z)\rho_\pm(z)\\&-\tfrac{1}{2}\rho_g^2\int_0^\infty dz\,t(z)+\tfrac{1}{2}\int_0^\infty dz\int_0^\infty dz'\delta\rho_\pm(z)\delta\rho_\pm(z')\hat{w}(|z-z'|)\\&+\rho_g\int_0^\infty dz[w_0-t(z)]\delta\rho_\pm(z)+\sigma_{gv} \ ,\end{aligned} \tag{A3}$$

where we have used the following notation:

$$\Delta f_{\text{HS}}(\rho_\pm(z),T)=f_{\text{HS}}(\rho_\pm(z),T)-f_{\text{HS}}(\rho_g,T) \ , \tag{A4}$$

$$\delta\rho_\pm(z)=\rho_\pm(z)-\rho_g \ , \tag{A5}$$

$$V_\pm(z)=V(x\to\pm\infty,z) \ , \tag{A6}$$

$$t(z)=\int_z^\infty dz'\hat{w}(z') \ , \tag{A7}$$

and

$$\hat{w}(z)=\int_{\mathbb{R}^2}d^2r\,\hat{w}((r^2+z^2)^{1/2}) \ . \tag{A8}$$

σ_{gv} is the artificial gas-vacuum surface tension due to the cutoff at $z=L_z$:

$$\sigma_{gv}=-\tfrac{1}{2}\rho_g^2\int_0^\infty dz\,t(z) \ . \tag{A9}$$

If the two parts of the substrate are identical, one has $\Omega_s^+(\rho_+(z))=\Omega_s^-(\rho_-(z))$ so that $\Omega_s^{\parallel}[\rho_+(z),\rho_-(z)]$ reduces to the expression for the surface free-energy density

$\Omega_s[\rho(z)]$ in the presence of a single homogeneous substrate [4]. The third term on the right-hand side of Eq. (2.2) takes the simple form

$$\Omega_s^{\perp}=2\sigma_{gv} \tag{A10}$$

with σ_{gv} given by Eq. (A9). This contribution is induced artificially by the lateral cutoff at $x=\pm L_x/2$.

The line contribution Ω_l can also be separated into an artificial ($\delta\Omega_l$) and into a physical ($\Omega_l^{(\mathrm{phys})}$) part

$$\Omega_l[\rho(x,z)]=\delta\Omega_l[\rho_+(z),\rho_-(z)]+\Omega_l^{(\mathrm{phys})}[\rho(x,z)] \ . \tag{A11}$$

$\delta\Omega_l[\rho_+(z),\rho_-(z)]$ depends only on the asymptotic profiles $\rho_{\pm}(z)$ and can be cast into the form

$$\delta\Omega_l[\rho_+(z),\rho_-(z)]=\tfrac{1}{2}\{\Delta\Omega_l[\rho_+(z)]+\Delta\Omega_l[\rho_-(z)]\} \ , \tag{A12}$$

where $\Delta\Omega_l[\rho(z)]$ is defined as

$$\begin{aligned}\Delta\Omega_l[\{\rho(z)\};T,\mu;\{w(r)\}]&=2\tau_{gvvv}-2\rho_g\int_0^{\infty}dz\,\delta\rho(z)\int_0^{\infty}dz'\,t(z')\\&+2\rho_g\int_0^{\infty}dx\int_0^{\infty}dz\,\rho(z)t(x,z)\\&-\int_0^{\infty}dz\int_0^{\infty}dz'\,\mathcal{W}(|z-z'|)\delta\rho(z)\delta\rho(z')\end{aligned} \tag{A13}$$

with

$$\mathcal{W}(z)=\int_0^{\infty}dx\int_x^{\infty}dx'\,\overline{w}(x',z) \tag{A14}$$

and the artificial line tension

$$\tau_{gvvv}=\tfrac{1}{2}\rho_g^2\Delta\tau \tag{A15}$$

is associated with a quarter space filled with gas in contact with three-quarter spaces of vacuum (see Appendix A in Ref. [19]);

$$\Delta\tau=\int_0^{\infty}dx\int_0^{\infty}dz\,t(x,z) \ , \tag{A16}$$

where

$$t(x,z)=\int_x^{\infty}dx'\int_z^{\infty}dz'\,\overline{w}(x',z') \ . \tag{A17}$$

The physically relevant contribution $\Omega_l^{(\mathrm{phys})}[\rho(x,z)]$ consist of two terms

$$\Omega_l^{(\mathrm{phys})}[\rho(x,z)]=\hat{\Omega}_l[\rho(x,z)]+\Delta\omega_l[\rho(x,z)] \ . \tag{A18}$$

The first term has a form similar to the surface contribution $\Omega_s(\rho(z))$ in Eq. (A3), but it depends, in addition, on the lateral variation of ρ:

$$\begin{aligned}\hat{\Omega}_l[\rho(x,z)]=&\int_{-\infty}^{\infty}dx\int_0^{\infty}dz[f_{\mathrm{HS}}(\rho(x,z),T)-f_{\mathrm{HS}}(\rho_{\infty}(x,z),T)]-\mu\int_{-\infty}^{\infty}dx\int_0^{\infty}dz\,\delta\rho(x,z)\\&+\int_{-\infty}^{\infty}dx\int_0^{\infty}dz\,V(x,z)\delta\rho(x,z)+\rho_g\int_{-\infty}^{\infty}dx\int_0^{\infty}dz[w_0-t(z)]\delta\rho(x,z)\\&+\tfrac{1}{2}\int_{-\infty}^{\infty}dx\int_{-\infty}^{\infty}dx'\int_0^{\infty}dz\int_0^{\infty}dz'\,\overline{w}(|x-x'|,|z-z'|)\delta\rho(x,z)\delta\rho(x',z') \ ,\end{aligned} \tag{A19}$$

where the asymptotic profiles $\rho_{\pm}(z)$ enter via

$$\delta\rho(x,z)=\rho(x,z)-\rho_{\infty}(x,z) \tag{A20}$$

and

$$\rho_{\infty}(x,z)=\Theta(-x)\rho_-(z)+\Theta(x)\rho_+(z) \ . \tag{A21}$$

The second contribution $\Delta\omega_l[\rho(x,z)]$ is given by

$$\begin{aligned}\Delta\omega_l[\rho(x,z)]=&\int_{-\infty}^{\infty}dx\int_0^{\infty}dz\,\delta V(x,z)\rho_{\infty}(x,z)\\&-\tfrac{1}{2}\int_0^{\infty}dz\int_0^{\infty}dz'[\delta\rho_+(z)-\delta\rho_-(z)][\delta\rho_+(z')-\delta\rho_-(z')]\mathcal{W}(|z-z'|)\\&+\int_{-\infty}^{\infty}dx\int_{-\infty}^{\infty}dx'\int_0^{\infty}dz\int_0^{\infty}dz'\,\overline{w}(|x-x'|,|z-z'|)\delta\rho(x,z)\delta\rho_{\infty}(x',z') \ .\end{aligned} \tag{A22}$$

Here we have used the notation

$$\delta\rho_{\infty}(x,z)=\rho_{\infty}(x,z)-\rho_g \tag{A23}$$

and

$$\delta V(x,z)=V(x,z)-V_{\infty}(x,z) \ , \tag{A24}$$

with

$$V_{\infty}(x,z)=\Theta(-x)V_-(z)+\Theta(x)V_+(z) \ . \tag{A25}$$

In the limit of a homogeneous substrate one has $\delta V(x,z)=0$, $\delta\rho(x,z)=0$ and $\delta\rho_+(z)=\delta\rho_-(z)$ so that the total line contribution $\Omega_l[\rho(x,z)]$ in Eq. (A11) reduces, as it should, to the artificial part $\Delta\Omega_l[\rho(z)]$ given by Eq. (A13).

At this point we want to remark that all the above artificial contributions have been also calculated *independently* for a finite fluid volume $L_x\times L_y\times L_z$ in contact with a semi-infinite homogeneous substrate. In this case

the physical part is given by the bulk (Ω_b) and the surface contribution ($\Omega_s^{\parallel}[\rho(z)]-\sigma_{gv}$); the artificial terms $[\sigma_{gv}+\Omega_s^{\perp}+\Delta\Omega_l[\rho(z)]]$ are due to the cutoff of the system at $x=\pm L_x/2$ and $z=L_z$. Even for such a comparably simple situation, the systematic identification and subsequent subtraction of artificial terms requires a careful analysis in order to be able to construct the correct expression for the surface free energy.

APPENDIX B: SURFACE AND LINE TENSIONS WITHIN THE SHARP-KINK APPROXIMATION

The bulk, surface, and line contributions within the sharp-kink approximation can be obtained as a special case by inserting the sharp-kink parametrization $\rho(x,z)=\hat{\rho}(x,z=l(x))$ [see Eq. (3.1)] into the corresponding expressions, which have been systematically derived in Appendix A as a functional for the full density distribution $\rho(x,z)$. The expressions for the surface and line tensions that are obtained by this specialization procedure are equal to those stemming from a straightforward calculation that starts directly from the grand-canonical density functional Ω given by Eq. (2.1) with $\rho(x,z)$ being replaced by $\hat{\rho}(x,z)$. This agreement forms a nontrivial cross-check for the results presented below.

Within the sharp-kink approximation [Eq. (3.1)] the decomposition of the grand-canonical free-energy functional $\Omega[\hat{\rho}(x,z)]$ given by Eq. (2.1) leads to explicit expressions for the surface ($\Omega_s^{\parallel}$ and $\Omega_s^{\perp}$) and line (Ω_l) contributions with the bulk contribution Ω_b given by Eq. (A1). $\Omega_s^{\parallel}$ has the form

$$\Omega_s^{\parallel}(l_+,l_-;\rho_l,\rho_g,T,\mu)=\tfrac{1}{2}\{\Omega_s^-(l_-)+\Omega_s^+(l_+)\} , \quad \text{(B1)}$$

where $\Omega_s^{\pm}(l_{\pm})$ corresponds to the effective interface potential of a homogeneous substrate w_+ and w_-, respectively (see Ref. [2])

$$\Omega_s^{\pm}(l)=l\Delta\Omega+\omega_{\pm}(l)+\sigma_{w_{\pm}l}+\sigma_{lg}+\sigma_{gv} \quad \text{(B2)}$$

with

$$\omega_{\pm}(l)=\Delta\rho\left[\int_{l-d_w^{\pm}}^{\infty}dz\,\rho_l t(z)-\int_l^{\infty}dz\,V_{\pm}(z)\right]$$
$$=a_2^{\pm}l^{-\sigma+1}+a_3^{\pm}l^{-\kappa+1}+\cdots , \quad l\gg d_w^{\pm} ; \quad \text{(B3)}$$

$a_2^{\pm}$ denotes the Hamaker constant in the presence of the substrate $\omega_{\pm}$. For nonretarded dispersion forces decaying $\sim r^{-(d+\sigma)}$ one typically has $\sigma=3$ and $\kappa=4$. σ_{gv} [see Eq. (A9) and the contribution 3 in Fig. 5] is the artificial gas-vacuum surface tension and $\Delta\rho=\rho_l-\rho_g$. [The contributions 5 in Fig. 5 are contained in $\Omega_s^{\perp}$ and are given by Eq. (A10).] The equilibrium wall-gas surface tension of a fluid exposed to semi-infinite homogeneous substrate w_+ and w_- is the minimum of $\Omega_s^{\pm}(l)-\sigma_{gv}$:

$$\sigma_{w_{\pm}g}=\min_l[\Omega_s^{\pm}(l)-\sigma_{gv}]=\Omega_s^{\pm}(\bar{l}_{\pm})-\sigma_{gv} . \quad \text{(B4)}$$

Within the sharp-kink approximation the liquid-vapor surface tension σ_{lg} is given by [4] (see 2 in Fig. 5)

$$\sigma_{lg}=-\tfrac{1}{2}(\Delta\rho)^2\int_0^{\infty}dz\,t(z) \quad \text{(B5)}$$

and the wall-liquid surface tension $\sigma_{w_{\pm}l}$ has, depending on the substrate, the form (see $1_{\pm}$ in Fig. 5)

$$\sigma_{w_{\pm}l}=\rho_l\int_{d_w^{\pm}}^{\infty}dx\,V_{\pm}(x)-d_w^{\pm}\Omega_b^{(l)}-\tfrac{1}{2}\rho_l^2\int_0^{\infty}dz\,t(z) . \quad \text{(B6)}$$

In Eq. (B2) the first term is determined by [compare Eq. (A1)]

$$\Delta\Omega=\Omega_b^{(l)}-\Omega_b^{(g)} , \quad \Omega_b^{(\gamma)}=\Omega_b(\rho_\gamma,T,\mu) . \quad \text{(B7)}$$

The surface free-energy density $\Omega_s^{\perp}$ is given by Eq. (A10). As in the case of the general density distribution, the line contribution $\Omega_l[l(x)]$ consists of two parts

$$\Omega_l[l(x)]=\delta\omega(l_+,l_-)+\Delta\omega[l(x)] . \quad \text{(B8)}$$

The first term $\delta\omega(l_+,l_-)$ contains all artificial contributions (σ_{lv} is defined analogously to σ_{gv} [Eq. (A9)]):

$$\delta\omega(l_+,l_-)=[(l_+-d_w^+)+(l_--d_w^-)]\sigma_{lv}$$
$$-(l_++l_-)\sigma_{gv}+2\tau_{gvvv}$$
$$+\delta\tau_+(l_+)+\delta\tau_-(l_-)$$
$$+\tau_{lw_+w_+v}+\tau_{lw_-w_-v}+2\tau_{lgvv} \quad \text{(B9)}$$

with

$$\tau_{lw_{\pm}w_{\pm}v}=\tfrac{1}{2}\rho_l^2\Delta\tau , \quad \text{(B10a)}$$

$$\tau_{gvvv}=\tfrac{1}{2}\rho_g^2\Delta\tau \quad \text{(B10b)}$$

(see II in Fig. 5),

$$\delta\tau_{\pm}(l_{\pm})=-\Delta\rho\rho_l\int_0^{\infty}dx\,T(x,l_{\pm}-d_w^{\pm}) , \quad \text{(B10c)}$$

and (see III in Fig. 5)

$$\tau_{lgvv}=\tfrac{1}{2}(\Delta\rho)^2\Delta\tau \quad \text{(B10d)}$$

[see Eqs. (A16) and (A17)] where $T(x,z)$ is given by Eq. (B15). The first four terms in Eq. (B9) correspond to the contributions 4 in Fig. 5 where $\delta\tau(l)$ denotes the interaction between the line contributions III and IV in Fig. 5 if l is finite. $\delta\tau(l)$ vanishes for $l\to\infty$ [see Eq. (B10c)]. $\tau_{lw_+w_+v}$, $\tau_{lw_-w_-v}$, τ_{gvvv}, and τ_{glvv} correspond to the contributions IV_+, IV_-, II, and III, respectively, in Fig. 5.

The physically relevant part of the line contribution itself consists of two parts

$$\Delta\omega[l(x)]=\omega_l(l_+,l_-)+\tilde{\omega}[l(x)] . \quad \text{(B11)}$$

The first term $\omega_l(l_+,l_-)$ depends only on the asymptotic values $l_{\pm}$, whereas the second one $\tilde{\omega}[l(x)]$ depends on the full shape of the profile of the liquid-vapor interface position $l(x)$:

$$\omega_l(l_+,l_-)=\tau_{lg}(l_+,l_-)+\tau_{lw_+w_-l} \quad \text{(B12)}$$

and

$$\tilde{\omega}[l(x)]=\Delta\Omega\Gamma_{\text{exch}}+\Delta\rho\rho_l\int_{-\infty}^{\infty}dx\,[T(l(x)-d_w^+)-T(l_\infty(x)-d_w^+)]-\Delta\rho\int_{-\infty}^{\infty}dx\,[U(x,l(x))-U(x,l_\infty(x))]$$
$$-\Delta\rho\rho_l\int_{-\infty}^{\infty}dx\,[T(x,l(x)-d_w^+)-T(x,l(x)-d_w^-)-T(x,l_\infty(x)-d_w^+)+T(x,l_\infty(x)-d_w^-)] \quad \text{(B13)}$$
$$-\tfrac{1}{2}(\Delta\rho)^2\int_{-\infty}^{\infty}dx\int_{-\infty}^{\infty}dx'\,\hat{w}(|x-x'|,l(x)-l(x'))\ ,$$

where

$$T(z)=\int_z^{\infty}dz'\,t(z')\ , \quad \text{(B14)}$$

$$T(x,z)=\int_z^{\infty}dz'\,t(x,z')\ , \quad \text{(B15)}$$

$$U(x,z)=\int_z^{\infty}dz'\,V(x,z')\ , \quad \text{(B16)}$$

and

$$\hat{w}(x,y)=\int_0^{\infty}dz\int_0^{y}dz'\,\bar{w}(x,|z-z'|)\ . \quad \text{(B17)}$$

$l_\infty(x)$ is defined via Eq. (3.9). For later purposes we introduce the analogous function

$$d_w^{\infty}(x)=\Theta(-x)d_w^-+\Theta(x)d_w^+\ . \quad \text{(B18)}$$

In Eq. (B12) we used the notations

$$\tau_{lg}(l_+,l_-)=-\Delta\rho\int_{-\infty}^{\infty}dx\,\delta U(x,l_\infty(x))-\Delta\rho\rho_l$$
$$\times\int_0^{\infty}dx\,[T(x,l_--d_w^-)-T(x,l_--d_w^+)$$
$$+T(x,l_+-d_w^+)-T(x,l_+-d_w^-)] \quad \text{(B19)}$$

and

$$\tau_{lw_+w_-l}=|d_w^+-d_w^-|\sigma_{lv}-\rho_l^2\int_0^{\infty}dx\,T(x,|d_w^+-d_w^-|)$$
$$+\tau_{lllv}+\tau_{vvvl}-\rho_l\int_{-\infty}^{\infty}dx\,\delta U(x,d_w^{\infty}(x))\ , \quad \text{(B20)}$$

where

$$\delta U(x,z)=\int_z^{\infty}dz'\delta V(x,z') \quad \text{(B21)}$$

with $\delta V(x,z)$ given by Eq. (A24). $\tau_{lw_+w_-l}$ is the line tension associated with the contact line between a semi-infinite *liquid* and the two adjacent substrate quarter spaces w_+ and w_- and therefore it is independent of l_+ and l_-. (This corresponds to the contribution V in Fig. 5.) τ_{lg} contains all those physical contributions to the line tension $\omega_l(l_+,l_-)$ that do depend on l_+ and l_-. In Eq. (B13) the difference in bulk-free energies is proportional to the quantity

$$\Gamma_{\text{exch}}=\int_{-\infty}^{\infty}dx\,[l(x)-l_\infty(x)]\ , \quad \text{(B22)}$$

which measures the exchange coverage, i.e., the difference in the area contained between the full profile $l(x)$ and the steplike profile $l_\infty(x)$ (see Fig. 5).

One can gain some insight into Eq. (B13) by considering the special case $l(x)=l_\infty(x)$, i.e., a steplike variation of the interfacial profile in the lateral direction (see Fig. 5). In this case $\tilde{\omega}[l]$, given by Eq. (B13), reduces to

$$\tilde{\omega}[l_\infty(x)]=\tau_{llllg}+\tau_{gggl}-(\Delta\rho)^2\int_0^{\infty}dx\int_{|l_+-l_-|}^{\infty}dz\,t(x,z)$$
$$+|l_+-l_-|\sigma_{lg} \quad \text{(B23)}$$

with

$$\tau_{llllg}=\tau_{gggl}=\tfrac{1}{2}(\Delta\rho)^2\Delta\tau \quad \text{(B24)}$$

[see Eqs. (A16), (A17), and (B5)]. In Eq. (B23) the first two terms correspond to the line tensions I_- and I_+ indicated in Fig. 5. For finite distances l_+-l_- the interaction between these two line contributions is described by the third term in Eq. (B23). The last term in Eq. (B23) is proportional to σ_{lg} and contributes to the surface tension of that part of the liquid-vapor interface that arises due to the steplike variation of $l(x)$ (see 2′ in Fig. 5).

The line tension τ of the system is given by the physical part of the line contribution $\Delta\omega[l(x)]$ [see Eq. (B11)], evaluated at the equilibrium values of l_+ and $l(x)$:

$$\tau=\omega_l(\bar{l}_+,\bar{l}_-)+\tilde{\omega}[\bar{l}(x)]\ . \quad \text{(B25)}$$

For the attractive part $\bar{w}(r)$ of the pair potential $w(r)$ [see Eq. (2.13)] the various auxiliary functions defined above can be computed analytically.

[1] D. E. Sullivan and M. M. Telo da Gama, in *Fluid Interfacial Phenomena,* edited by C. A. Croxton (Wiley, New York, 1986), p. 45.

[2] S. Dietrich, in *Phase Transitions and Critical Phenomena,* edited by C. Domb and J. L. Lebowitz (Academic, London, 1988), Vol. 12, p. 1.

[3] M. Schick, in *Liquids at Interfaces,* Proceedings of the Les Houches Summer of School of Theoretical Physics, Session XLVIII, edited by J. Chavrolin, J. F. Joanny, and J. Zinn-Justin (Elsevier, Amsterdam, 1990), p. 415.

[4] S. Dietrich and M. Napiórkowski, Phys. Rev. A **43**, 1861 (1991).

[5] S. Dietrich, in *Phase Transitions in Surface Films 2,* Vol. 267 of *NATO Advanced Study Institute Series B: Physics,* edited by H. Taub, G. Torzo, H. J. Lauter, and S. C. Fain (Plenum, New York, 1991), p. 391.

[6] E. Cheng, M. W. Cole, and A. L. Stella, Europhys. Lett. **8**, 527 (1989).

[7] P. Pfeifer, Y. J. Wu, M. W. Cole, and J. Krim, Phys. Rev. Lett. **62**, 1997 (1989).
[8] M. Kardar and J. O. Indekeu, Europhys. Lett. **12**, 161 (1990).
[9] G. Guigliarelli and A. L. Stella, Phys. Scr. **T35**, 34 (1991).
[10] D. Andelman, J. F. Joanny, and M. O. Robbins, Europhys. Lett. **7**, 731 (1988).
[11] E. V. Albano, K. Binder, D. W. Heermann, and W. Paul, Surf. Sci. **223**, 151 (1989).
[12] E. V. Albano, K. Binder, D. W. Heerman, and W. Paul, Z. Phys. B **47**, 445 (1989).
[13] A. C. Levi and E. Tosatti, Surf. Sci. **178**, 425 (1986).
[14] G. Bilalbegović, V. Privman, and N. M. Švrakić, J. Phys. A **22**, L833 (1989).
[15] B. V. Derjaguin and N. V. Churaev, J. Colloid Interface Sci. **54**, 157 (1976).
[16] Y. Pomeau, J. Colloid Interface Sci. **113**, 5 (1985).
[17] E. Cheng and M. W. Cole, Phys. Rev. B **41**, 9650 (1990).
[18] P. M. Duxbury and A. C. Orrick, Phys. Rev. B **39**, 2944 (1989).
[19] M. Napiórkowski, W. Koch, and S. Dietrich, Phys. Rev. A **45**, 5760 (1992).
[20] E. H. Hauge, Phys. Rev. A **46**, 4994 (1992).
[21] M. W. Cole and E. Vittorators, J. Low Temp. Phys. **22**, 223 (1976).
[22] P. G. de Gennes, Rev. Mod. Phys. **64**, 645 (1992).
[23] C. Casagrande and M. Veyssié, C. R. Acad. Sci. (Paris) **II-306**, 1423 (1988).
[24] E. Raphaël, C. R. Acad. Sci. France **II-307**, 9 (1988).
[25] C. Casagrande, P. Fabre, E. Raphaël, and M. Veyssié, Europhys. Lett. **9**, 251 (1989).
[26] T. Ondarçuhu, P. Fabre, E. Raphaël, and M. Veyssié, J. Phys. (Paris) **51**, 1527 (1990).
[27] E. Raphaël, C. R. Acad. Sci. (Paris) **II-306**, 751 (1988).
[28] T. Ondarçuhu and M. Veyssié, J. Phys. II **1**, 75 (1991).
[29] T. Ondarçuhu and E. Raphaël, C. R. Acad. Sci. (Paris) **II-314**, 453 (1992).
[30] M. O. Robbins, D. Andelman, and J. F. Joanny, Phys. Rev. A **43**, 4344 (1991).
[31] C. Sykes, C. R. Acad. Sci. (Paris) **II-313**, 607 (1991).
[32] L. Łajtar and S. Sokołowski, J. Chem. Soc. Faraday Trans. **88**, 2545 (1992).
[33] J.-O. Carlson, Crit. Rev. Solid State Mater. Sci. **16**, 161 (1990).
[34] C. Chmiel, K. Karykowski, A. Patrykiejew, W. Rżysko, and S. Sokołowski, Mol. Phys. **81**, 691 (1994).
[35] W. Gaz. A. Patrykiejew, and S. Sokołowksi, Surf. Sci. **306**, 434 (1994).
[36] J. O. Indekeu, Physica A **183**, 439 (1992).
[37] R. Evans, Adv. Phys. **28**, 143 (1979).
[38] J. D. Weeks, D. Chandler, and H. C. Andersen, J. Chem. Phys. **54**, 5237 (1971).
[39] P. Tarazona and R. Evans, Mol. Phys. **48**, 799 (1983).
[40] T. Aukrust and E. H. Hauge, Physica A **141**, 427 (1987).
[41] N. F. Carnahan and K. E. Starling, J. Chem. Phys. **51**, 635 (1969).
[42] *Handbook of Mathematical Functions,* edited by M. Abramowitz and I. A. Stegun (Dover, New York, 1972).
[43] J. F. Joanny and P. G. de Gennes, J. Chem. Phys. **81**, 552 (1984).
[44] Y. Pomeau and J. Vannimenus, J. Colloid Interface Sci. **104**, 477 (1985).
[45] H. W. Diehl, in *Phase Transitions and Critical Phenomena,* edited by C. Domb and J. L. Lebowitz (Academic, London, 1986), Vol. 10, p. 217.
[46] H. W. Diehl and M. Smock, Phys. Rev. B **47**, 5841 (1993); **48**, 6740(E) (1993).
[47] M. Smock, H. W. Diehl, and D. P. Landau, Ber. Bunseng. Phys. Chem. **98**, 486 (1994).
[48] A. Robledo and J. O. Indekeu, Europhys. Lett. **25**, 17 (1994).
[49] S. Dietrich and M. Napiórkowski, Physica A **177**, 437 (1991).
[50] M. Napiórkowski and S. Dietrich, Z. Phys. B **89**, 263 (1992).
[51] M. Napiórkowski and S. Dietrich, Phys. Rev. E **47**, 1836 (1993).
[52] P. G. de Gennes, Rev. Mod. Phys. **57**, 827 (1985).
[53] The comparison of our algorithm with a library routine for selected values of parameters revealed negligible numerical deviations of about $10^{-12}\sigma$ in $\bar{l}(x)$ for all values of x whereby our algorithm was ten times faster. In our actual calculations we required an accuracy of $10^{-6}\sigma$.
[54] J. O. Indekeu, Int. J. Mod. Phys. B **8**, 309 (1994); J. O. Indekeu and H. T. Dobbs, J. Phys. (France) I **4**, 77 (1994).
[55] T. Getta and S. Dietrich, Phys. Rev. E **47**, 1856 (1993).
[56] J. Gaydos and A. W. Neumann, J. Colloid Interface Sci. **120**, 76 (1987).
[57] D. Li and A. W. Neumann, Colloid Surf. **43**, 307 (1990).
[58] J. Drelich, J. D. Miller, and J. Hupka, J. Colloid Interface Sci. **155**, 379 (1993).